Nuclearity Controlled Cyanide-Bridged Bimetallic Cr^{III}–Mn^{II} Compounds: Synthesis, Crystal Structures, Magnetic Properties and Theoretical Calculations

Luminita Toma,[a] Rodrigue Lescouëzec,[a] Jacqueline Vaissermann,[b] Fernando S. Delgado,[c] Catalina Ruiz-Pérez,[c] Rosa Carrasco,[a] Juan Cano,[a] Francesc Lloret,[a] and Miguel Julve*[a]

Abstract: The preparation, X-ray crystallography and magnetic investigation of the compounds PPh_4-$[Cr(bipy)(CN)_4]\cdot 2\,CH_3CN\cdot H_2O$ (**1**) (mononuclear), $[\{Cr(bipy)(CN)_4\}_2Mn(H_2O)_4]\cdot 4\,H_2O$ (**2**) (trinuclear), $[\{Cr(bipy)(CN)_4\}_2Mn(H_2O)_2]$ (**3**) (chain) and $[\{Cr(bipy)(CN)_4\}_2Mn(H_2O)]\cdot H_2O\cdot CH_3CN$ (**4**) (double chain) [bipy = 2,2′-bipyridine; PPh_4^+ = tetraphenylphosphonium] are described herein. The $[Cr(bipy)(CN)_4]^-$ unit act either as a monodentate (**2**) or bis-monodentate (**3**) ligand toward the manganese atom through one (**2**) or two (**3**) of its four cyanide groups. The manganese atom is six-coordinate with two (**2**) or four (**3**) cyanide nitrogens and four (**2**) or two (**3**) water molecules building a distorted octahedral environment. In **4**, two chains of **3** are pillared through interchain Mn-N-C-Cr links which replace one of the two *trans*-coordinated water molecules at the manganese atom to afford a double chain structure where bis- and tris-monodenate coordination modes of $[Cr(bipy)(CN)_4]^-$ coexist. The magnetic properties of **1**–**4** were investigated in the temperature range 1.9–300 K. A Curie law behaviour for a magnetically isolated spin quartet is observed for **1**. A significant antiferromagnetic interaction between Cr^{III} and Mn^{II} through the single cyanide bridge [$J = -6.2\ cm^{-1}$, the Hamiltonian being defined as $\hat{H} = -J(\hat{S}_{Cr(1)}\cdot\hat{S}_{Mn}+\hat{S}_{Cr(2)}\cdot\hat{S}_{Mn})$] occurs in **2** leading to a low-lying spin doublet which is fully populated at $T < 5$ K. A metamagnetic behaviour is observed for **3** and **4** [the values of the critical field H_c being ca. 3000 (**3**) and 1500 Oe (**4**)] which is associated to the occurrence of weak interchain antiferromagnetic interactions between ferrimagnetic $Cr^{III}_2Mn^{II}$ chains. The analysis of the exchange pathways in **2**–**4** through DFT type calculations together with the magnetic bevaviour simulation using the quantum Monte Carlo methodology provided a good understanding of their magnetic properties.

Keywords: bimetallic chains · crystal engineering · cyanides · magnetic properties · polynuclear complexes

Introduction

In recent years, there has been an impressive body of publications dealing with the self-assembly of cyano-linked metal complexes.[1–6] The main synthetic route which is currently employed consists of using a stable cyanometallate anion as a ligand toward either fully solvated metal ions or preformed complexes whose coordination sphere is unsaturated (presence of some coordination sites which are filled by solvent molecules). The highly insoluble three-dimensional Prussian Blue analogues are obtained when the cyanide-bearing complex is the hexacyanometallate anion $[M(CN)_6]^{3-}$ and the cation is the unprotected fully solvated species.[2] Lower dimensionality heterometallic compounds with very different topologies and structures result if the outer metal ions are partially blocked with polydentate ligands.[3–5] This structural diversity associated to their inter-

[a] L. Toma, Dr. R. Lescouëzec, Dr. R. Carrasco, Dr. J. Cano, Prof. F. Lloret, Prof. M. Julve
Departament de Química Inorgànica/Instituto de Ciencia Molecular
Facultat de Química de la Universitat de València
Avda. Dr. Moliner 50, 46100 Burjassot, València (Spain)
Fax.: (+34) 96-354-4322
E-mail: miguel.julve@uv.es

[b] Dr. J. Vaissermann
Laboratoire de Chimie Inorganique et Matériaux Moléculaires
CNRS, UMR 7071, Université Pierre et Marie Curie
75252 Paris Cedex 05 (France)

[c] F. S. Delgado, Prof. C. Ruiz-Pérez
Laboratorio de Rayos X y Materiales Moleculares
Departamento de Física Fundamental II
Universidad de La Laguna
380204 La Laguna, Tenerife (Spain)

Supporting information for this article is available on the WWW under http://www.chemeurj.org/ or from the author.

  DOI: 10.1002/chem.200400611

esting properties such as hosts for small molecules and ions,[1,7] catalysts for the production of ether polyols or polycarbonates,[8] room temperature magnets,[9–11] high spin molecules,[5,12] single-molecule magnets,[13] electrochemically tunable magnets[14] or photo-magnetic materials[14b,15] account for the great number of publications dealing with cyanide-bridged heterometallic species.

Our research team, among others, is engaged in the design and use as ligands of new stable cyanide-bearing six-coordinate complexes of general formula $[ML(CN)_x]^{(x+l-3)-}$ (M = trivalent first row transition metal ion) where the overall charge and the number of cyanide ligands depend on the charge and denticity of the polydentate L ligand.[16–23] The possibilities offered by this type of precursors in preparative chemistry and the relevant parameters to be taken into account are summarized in Scheme 1. One can see there how the nature, denticity and charge of L are crucial parameters given the possibility of supramolecular interactions (case of aromatic L groups), the control of the stereochemistry (*fac*- or *mer*- arrangement of the three cyanide groups when L is a tridentate ligand) or the selective complexation (L being a bridging ligand in addition to the cyanide groups). In order to illustrate the new magneto-structural possibilities that this strategy can afford and restricting ourselves to very recent results that we got with the use of the mononuclear low-spin iron(III) precursors $[Fe(bipy)(CN)_4]^-$ (bipy = 2,2′-bipyridine), $[Fe(phen)(CN)_4]^-$ (phen = 1,10-phenanthroline), *fac*-$[Fe\{HB(pz)_3\}(CN)_3]^-$ [$HB(pz)_3$ = hydrotris(1-pyrazolyl)borate anion] and *mer*-$[Fe(bpca)(CN)_3]^-$ [bpca = bis(2-pyridylcarbonyl)amidate] as ligands, the following findings can be outlined: i) the tetranuclear iron(III) compound *fac*-$\{[Fe\{HB(pz)_3\}(CN)_3]_3Fe(H_2O)_3\}\cdot 6H_2O$ where the ferromagnetic coupling between the three low-spin iron(III) *fac*-$[Fe\{HB(pz)_3\}(CN)_3]^-$ peripheral units and the central high-spin iron(III) $[Fe(H_2O)_3]^{3+}$ entity through single cyanide bridges leads to a low-lying nonet spin sate;[24] ii) the ferromagnetic chains $[\{FeL(CN)_4\}_2Co(H_2O)_2]\cdot 4H_2O$ (L = bipy and phen) which exhibit slow magnetic relaxation and hysteresis effects and thus are among the scarce examples of single chain magnets (SCM);[25,26] iii) the double chain $[\{FeL(CN)_4\}_2Co(H_2O)]\cdot CH_3CN\cdot {}^1/_2H_2O$ where two of the previous ferromagnetic chains are condensed through the loss of a coordinated water molecule from cobalt(II) and its replacement by a cyanide bridge, the whole exhibiting a metamagnetic behaviour;[27] iv) the ferrimagnetic ladder-like bimetallic chain $\{[Fe(bpca)(\mu\text{-}CN)_3Mn(H_2O)_3]\cdot[Fe(bpca)(CN)_3]\}\cdot 3H_2O$ which exhibits ferrimagnetic ordering below 2.0 K.[28]

In the present paper, we extend these studies to a new building block of formula $[Cr(bipy)(CN)_4]^-$ which is isolated as a tetraphenylphosphonium salt (**1**). The fact that the chromium(III) ion in **1** has three unpaired electrons against only one in the case of the related low-spin iron(III) derivative demonstrates the general character and validity of the approach sketched in Scheme 1. The use of the mononuclear $[Cr(bipy)(CN)_4]^-$ unit of **1** as a ligand towards $[Mn(H_2O)_6]^{2+}$ afforded the trinuclear compound $[\{Cr(bipy)(CN)_4\}_2Mn(H_2O)_4]\cdot 4H_2O$ (**2**), the zigzag chain $[\{Cr(bipy)(CN)_4\}_2Mn(H_2O)_2]$ (**3**) and the double chain $[\{Cr(bipy)(CN)_4\}_2Mn(H_2O)]\cdot H_2O\cdot CH_3CN$ (**4**). The preparation and magneto-structural investigation of these four compounds are reported here.

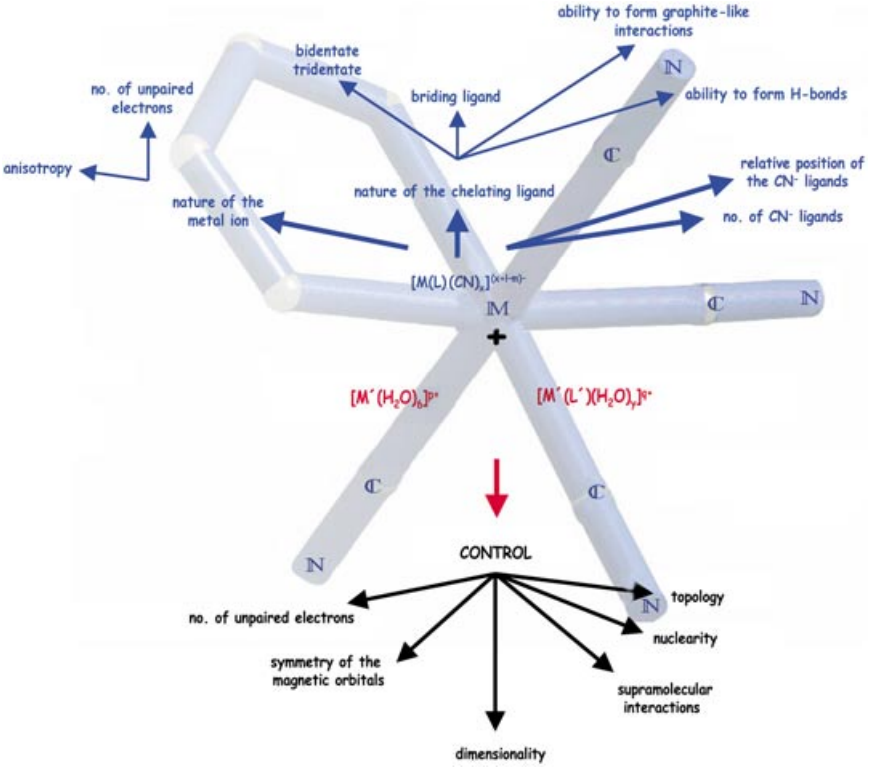

Scheme 1.

Results and Discussion

Description of the structures: The structures of the compounds **1**–**4** have been characterised by single crystal X-ray diffraction. Their crystallographic data and the details of the refinements have been deposited at the Cambridge Crystallographic Data Centre and they are reported in a condensed form in Table 1. The key distances and angles are reported in Table 2 (**1**), Table 3 (**2**), Table 4 (**3**) and Table 5 (**4**).

$PPh_4[Cr(bipy)(CN)_4]\cdot 2CH_3CN\cdot H_2O$ (1): The crystallographic analysis of **1** shows that its structure consists of mononuclear $[Cr(bipy)(CN)_4]^-$ anions (Figure 1), tetraphenylphosphonium cations and uncoordinated water and acetonitrile molecules. The anions are grouped

Table 1. Crystallographic data and structure refinement for $PPh_4[Cr(bipy)(CN)_4]\cdot 2CH_3CN\cdot H_2O$ (**1**), $[\{Cr(bipy)(CN)_4\}_2Mn(H_2O)_4]\cdot 4H_2O$ (**2**), $[\{Cr(bipy)(CN)_4\}_2Mn(H_2O)_2]$ (**3**) and $[\{Cr(bipy)(CN)_4\}_2Mn(H_2O)]\cdot H_2O\cdot CH_3CN$ (**4**).

Compound	**1**	**2**	**3**	**4**
chemical formula	$C_{42}H_{36}CrN_8OP$	$C_{28}H_{32}Cr_2MnN_{12}O_8$	$C_{28}H_{20}Cr_2MnN_{12}O_2$	$C_{30}H_{23}Cr_2MnN_{13}O_2$
F_w	751.77	823.56	715.47	756.55
crystal system	triclinic	monoclinic	monoclinic	monoclinic
a [Å]	8.144(4)	11.859(6)	7.894(4)	20.232(4)
b [Å]	14.494(3)	13.580(9)	15.171(8)	7.608(2)
c [Å]	17.149(7)	11.854(6)	12.640(4)	21.486(4)
α [°]	80.52(3)	90	90	90
β [°]	87.80(4)	100.51(4)	94.45(3)	96.43(3)
γ [°]	87.02(3)	90	90	90
V [Å^3]	1993(1)	1877(2)	722	3286.4(12)
Z	2	2	2	4
T [K]	295	295	295	293
space group	$P(-1)$	$P2_1/c$	$P2_1/n$	$P2_1/n$
$F(000)$	782	842	722	1532
$\mu(Mo_{K\alpha})$ [cm^{-1}]	3.70	9.60	11.68	10.78
no. parameters	479	234	2.07	433
max/min transmission	1.00/0.83	0.87/0.54	1.00/0.84	
index ranges				
	$-9\le h\le 10$	$-14\le h\le 13$	$-9\le h\le 9$	$24\le h\le 28$
	$-17\le k\le 17$	$0\le k\le 16$	$0\le k\le 18$	$-10\le k\le 8$
	$0\le l\le 21$	$-0\le l\le 16$	$0\le l\le 15$	$-26\le l\le 30$
measured reflns	8365	3620	2972	9147
θ range [°]	1–26	1–25	1–25	6.45–30
obsd reflns	7781	3286	2647	5256
largest peak/hole [e Å^{-3}]	0.40/−0.36	0.73/−0.49	0.93/−0.87	0.93/−0.47
final R indices		$[I > 3\sigma(I)]$		$[I > 2\sigma(I)]$
R[a]	0.045	0.057	0.057	0.0585
R_w	0.053[b]	0.067[b]	0.070[b]	0.111[c]
goodness-of-fit	1.123	1.097	1.024	0.974

[a] $R=\Sigma(||F_o|-|F_c||)/\Sigma|F_o|$. [b] $R_w=[\Sigma\{(|F_o|-|F_c|)^2/\Sigma\}|F_o|^2]^{1/2}$. [c] $R_w=[\Sigma\{(|F_o|^2-|F_c|^2)^2/\Sigma\}|F_o|^2]^{1/2}$.

Table 2. Selected bond lengths [Å] and angles [°] in complex **1**.

Cr(1)−N(11)	2.079(3)	Cr(1)−N(12)	2.073(3)
Cr(1)−C(1)	2.064(4)	Cr(1)−C(2)	2.051(3)
Cr(1)−C(3)	2.055(4)	Cr(1)−C(4)	2.076(4)
C(1)−N(1)	1.149(5)	C(2)−N(2)	1.139(5)
C(3)−N(3)	1.135(5)	C(4)−N(4)	1.136(5)
N(11)-Cr(1)-N(12)	78.73(11)	N(11)-Cr(1)-C(1)	91.99(12)
N(11)-Cr(1)-C(2)	173.15(14)	N(11)-Cr(1)-C(3)	93.91(13)
N(11)-Cr(1)-C(4)	88.71(12)	N(12)-Cr(1)-C(1)	90.35(13)
N(12)-Cr(1)-C(2)	94.96(13)	N(12)-Cr(1)-C(3)	172.56(13)
N(12)-Cr(1)-C(4)	88.55(13)	C(1)-Cr(1)-C(2)	90.72(14)
C(1)-Cr(1)-C(3)	91.02(15)	C(1)-Cr(1)-C(4)	178.56(14)
C(2)-Cr(1)-C(3)	92.33(15)	C(2)-Cr(1)-C(4)	88.45(14)
C(3)-Cr(1)-C(4)	90.19(15)	Cr(1)-C(1)-N(1)	178.8(3)
Cr(1)-C(2)-N(2)	178.4(4)	Cr(1)-C(3)-N(3)	178.6(3)
Cr(1)-C(4)-N(4)	178.1(3)		

Table 3. Selected bond lengths [Å] and angles [°] in complex **2**.[a]

Cr(1)−N(11)	2.059(5)	Cr(1)−N(12)	2.080(5)
Cr(1)−C(1)	2.068(7)	Cr(1)−C(2)	2.058(7)
Cr(1)−C(3)	2.049(8)	Cr(1)−C(4)	2.041(8)
Mn(1)−O(1)	2.192(5)	Mn(1)−O(2)	2.200(6)
Mn(1)−N(1)	2.215(6)	C(1)−N(1)	1.142(9)
C(2)−N(2)	1.142(9)	C(3)−N(3)	1.156(9)
C(4)−N(4)	1.160(9)		
N(11)-Cr(1)-N(12)	79.36(19)	N(11)-Cr(1)-C(1)	170.2(2)
N(11)-Cr(1)-C(2)	95.1 (2)	N(11)-Cr(1)-C(3)	89.7(2)
N(11)-Cr(1)-C(4)	89.0(2)	N(12)-Cr(1)-C(1)	92.6(2)
N(12)-Cr(1)-C(2)	172.9(3)	N(12)-Cr(1)-C(3)	88.9(2)
N(12)-Cr(1)-C(4)	93.7(2)	C(1)-Cr(1)-C(2)	93.3(3)
C(1)-Cr(1)-C(3)	95.9(3)	C(1)-Cr(1)-C(4)	85.8(3)
C(2)-Cr(1)-C(3)	86.7 (3)	C(2)-Cr(1)-C(4)	90.6(3)
C(3)-Cr(1)-C(4)	176.9(3)	O(1)-Mn(1)-O(2)	90.3(2)
O(1)-Mn(1)-O(2a)	89.7(2)	O(1)-Mn(1)-N(1)	85.8(2)
O(1)-Mn(1)-N(1a)	94.2(2)	O(2)-Mn(1)-N(1)	92.0(2)
O(2)-Mn(1)-N(1a)	88.0(2)	Cr(1)-C(1)-N(1)	170.7(7)
Cr(1)-C(2)-N(2)	176.6(9)	Cr(1)-C(3)-N(3)	175.3(7)
Cr(1)-C(4)-N(4)	177.9(6)	Mn(1)-N(1)-C(1)	168.9(6)

[a] Symmetry code: a = $1-x$, $1-y$, $1-z$.

values of the Cr−N(bipy) bond lengths [2.079(3) and 2.073(3) Å for Cr(1)−N(11) and Cr(1)−N(12) agree with those previously reported for other bipy-containing chromium(III) complexes.[29] This agreement is also observed between the Cr–C(cyano) bond lenghts of **1** [2.076(4)–2.051(3) Å] and those reported for the hexacyanochromate(III) unit in the ionic salts of formula $K_3[Cr(CN)_6]$ [2.100(10)–2.057(12 Å],[30] $(NMe_4)_2A[Cr(CN)_6]$ with A = K^+ [mean value 2.093(2) Å][31] and Cs^+ [av. value 2.061(6) Å][31] and $Ba_3[Cr(CN)_6]\cdot 20H_2O$ [av. value 2.069(5) Å].[31] The Cr(1)-C-N angles for the terminally bound cyanide ligands in **1** are quasi-linear [178.8(3)–178.1(3)°]. The values of the cyanide C–N bonds vary in the range 1.149(5)–1.135(5) Å. The occurrence of uncoordinated acetonitrile molecules and terminally bound cyanide groups in the structure of **1** is consistent with the presence of two cyanide stretching vibrations at 2212(w) (CH_3CN solvent molecule) and 2124(w) cm^{-1} (monodentate cyanide).

by pairs through hydrogen bonds involving the crystallization water molecule [O(1)] and two cyanide-nitrogen atoms [N(3) and N(4a)] from two $[Cr(bipy)(CN)_4]^-$ units (Figure S1, Supporting Information) resulting in a quasi-square centrosymmetric Cr(1)-O(1)-Cr(1a)-O(1a) motif [2.975(5) and 2.857(5) Å for N(3)···O(1) and N(4)···O(1a), respectively; a = $-x$, $1-y$, $1-z$].

Each chromium atom is six-coordinated with two bipy-nitrogen atoms and four cyanide-carbon atoms in a distorted octahedral geometry. The short bite angle of the chelating bipy [78.73(11)° for N(11)-Cr(1)-N(12)] is the main factor accounting for this distortion from the ideal geometry. The

Bond lengths and angles within this ligand are in agreement with those reported for free bipy.[32] No significant π–π staking interactions between adjacent bipy ligands are observed. The bulky tetraphenylphophosphonium cation ex-

Table 4. Selected bond lengths [Å] and angles [°] in complex **3**.[a]

Cr(1)–N(11)	2.060(4)	Cr(1)–N(12)	2.059(5)
Cr(1)–C(1)	2.057(6)	Cr(1)–C(2)	2.037(6)
Cr(1)–C(3)	2.079(6)	Cr(1)–C(4)	2.050(6)
Mn(1)–N(1)	2.245(5)	Mn(1)–N(3b)	2.222(5)
Mn(1)–O(1)	2.179(4)	C(1)–N(1)	1.146(7)
C(2)–N(2)	1.134(8)	C(3)–N(3)	1.132(7)
C(4)–N(4)	1.133(8)		
N(11)-Cr(1)-N(12)	78.66(17)	N(11)-Cr(1)-C(1)	171.65(19)
N(11)-Cr(1)-C(2)	93.64(19)	N(11)-Cr(1)-C(3)	92.02(19)
N(11)-Cr(1)-C(4)	92.1(2)	N(12)-Cr(1)-C(1)	94.24(19)
N(12)-Cr(1)-C(2)	172.30(19)	N(12)-Cr(1)-C(3)	89.35(19)
N(12)-Cr(1)-C(4)	90.55(19)	C(1)-Cr(1)-C(2)	93.5(2)
C(1)-Cr(1)-C(3)	92.3(2)	C(1)-Cr(1)-C(4)	83.5(2)
C(2)-Cr(1)-C(3)	90.7 (2)	C(2)-Cr(1)-C(4)	90.0(2)
C(3)-Cr(1)-C(4)	175.8(2)	N(1)-Mn(1)-N(3b)	92.12(18)
N(1)-Mn(1)-N(3c)	87.88(18)	N(1)-Mn(1)-O(1)	86.40(17)
N(1)-Mn(1)-O(1a)	93.60(17)	N(3b)-Mn(1)-O(1)	84.02(17)
N(3c)-Mn(1)-O(1)	95.98(17)	Cr(1)-C(1)-N(1)	169.6(5)
Cr(1)-C(2)-N(2)	174.9(5)	Cr(1)-C(3)-N(3)	172.7(5)
Cr(1)-C(4)-N(4)	172.3(5)	Mn(1)-N(1)-C(1)	140.5(4)
Mn(1)-N(3b)-C(3b)	139.6(5)		

[a] Symmetry code: a = $1-x, -y, 1-z$; b = $1+x, y, z$; c = $-x, -y, 1-z$.

Table 5. Selected bond lengths [Å] and angles [°] in complex **4**.[a]

Cr(1)–N(11)	2.056(3)	Cr(1)–N(12)	2.063(3)
Cr(1)–C(1)	2.065(3)	Cr(1)–C(2)	2.056(3)
Cr(1)–C(3)	2.084(3)	Cr(1)–C(4)	2.047(3)
Cr(2)–N(21)	2.049(3)	Cr(2)–N(22)	2.065(3)
Cr(2)–C(5)	2.048(4)	Cr(2)–C(6)	2.046(4)
Cr(2)–C(7)	2.083(3)	Cr(2)–C(8)	2.066(4)
Mn(1)–N(1)	2.203(3)	Mn(1)–N(2a)	2.199(3)
Mn(1)–N(3b)	2.209(3)	Mn(1)–N(5)	2.223(3)
Mn(1)–N(7c)	2.208(3)	Mn(1)–O(1w)	2.388(3)
C(1)–N(1)	1.148(5)	C(2)–N(2)	1.139(5)
C(3)–N(3)	1.142(5)	C(4)–N(4)	1.140(5)
C(5)–N(5)	1.136(5)	C(6)–N(6)	1.146(6)
C(7)–N(7)	1.146(5)	C(8)–N(8)	1.141(6)
N(11)-Cr(1)-N(12)	78.4(1)	N(11)-Cr(1)-C(1)	175.4(1)
N(11)-Cr(1)-C(2)	95.35(1)	N(11)-Cr(1)-C(3)	89.09(1)
N(11)-Cr(1)-C(4)	89.5(1)	N(12)-Cr(1)-C(1)	97.3(1)
N(12)-Cr(1)-C(2)	170.6(6)	N(12)-Cr(1)-C(3)	96.6(1)
N(12)-Cr(1)-C(4)	87.1(1)	C(1)-Cr(1)-C(2)	89.1(1)
C(1)-Cr(1)-C(3)	90.0(1)	C(1)-Cr(1)-C(4)	91.7(1)
C(2)-Cr(1)-C(3)	90.2(1)	C(2)-Cr(1)-C(4)	85.8(1)
C(3)-Cr(1)-C(4)	175.7(1)	N(21)-Cr(22)-N(22)	78.6(1)
N(21)-Cr(2)-C(5)	96.6(1)	N(21)-Cr(2)-C(6)	175.1(1)
N(21)-Cr(2)-C(7)	91.5(1)	N(21)-Cr(2)-C(8)	92.3(1)
N(22)-Cr(2)-C(5)	171.8(1)	N(22)-Cr(2)-C(6)	97.2(1)
N(22)-Cr(2)-C(7)	97.1(1)	N(22)-Cr(2)-C(8)	88.2(1)
C(5)-Cr(2)-C(6)	87.7(1)	C(5)-Cr(2)-C(7)	89.7(1)
C(5)-Cr(2)-C(8)	85.2(1)	C(6)-Cr(2)-C(7)	86.5(1)
C(6)-Cr(2)-C(8)	90.1(1)	C(7)-Cr(2)-C(8)	173.9(1)
O(1w)-Mn(1)-N(1)	172.8(1)	O(1w)-Mn(1)-N(2a)	82.71(1)
O(1w)-Mn(1)-N(3b)	92.53(1)	O(1w)-Mn(1)-N(5)	82.8(1)
O(1w)-Mn(1)-N(7c)	78.51(1)	N(1)-Mn(1)-N(2a)	97.19(1)
N(1)-Mn(1)-N(3b)	94.63(1)	N(1)-Mn(1)-N(5)	90.0(1)
N(1)-Mn(1)-N(7c)	101.57(1)	N(2a)-Mn(1)-N(3b)	89.33(1)
N(2a)-Mn(1)-N(5)	87.25(1)	N(2a)-Mn(1)-N(7c)	161.19(1)
N(3b)-Mn(1)-N(5)	174.55(1)	N(3b)-Mn(1)-N(7c)	90.46(1)
N(5)-Mn(1)-N(7c)	91.41(1)	Cr(1)-C(1)-N(1)	176.5(3)
Cr(1)-C(2)-N(2)	176.0(3)	Cr(1)-C(3)-N(3)	173.9(3)
Cr(1)-C(4)-N(4)	175.7(3)	Cr(2)-C(5)-N(5)	171.0(3)
Cr(2)-C(6)-N(6)	176.5(3)	Cr(2)-C(7)-N(7)	175.1(3)
Cr(2)-C(8)-N(8)	176.9(3)	Mn(1)-N(1)-C(1)	174.1(3)
Mn(1)-N(2a)-C(2a)	176.02(3)	Mn(1)-N(3b)-C(3b)	175.25(3)
Mn(1)-N(5)-C(5)	146.8(3)	Mn(1)-N(7c)-C(7c)	169.82(3)

[a] Symmetry code: a = $^3/_2-x, -^1/_2+y, ^1/_2-z$; b = $^3/_2-x, ^1/_2+y, ^1/_2-z$; c = $x, 1+y, z$.

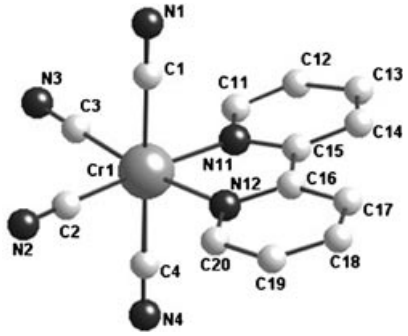

Figure 1. Perspective drawing of the $[Cr(bipy)(CN)_4]^-$ anion of complex **1** showing the atom numbering. The hydrogen atoms of bipy have been omitted for the sake clarity.

hibits the expected tetrahedral shape and its bond lengths and angles are as expected. Interestingly, the PPh_4^+ cations are grouped by pairs along the *b* axis, the resulting motif being the parallel quadrupole phenyl embrace (PQPE)[33] with a P···P separation of 8.19 Å (Figure S2). Regular alternating of two kind of layers growing in the *ab* plane [hydrophobic cationic (tetraphenylphosphonium) and hydrophilic anionic (pairs of $[Cr(bipy)(CN)_4]^-$] which are held by two water molecules occur in the unit cell (Figure S2). The value of the shortest intermolecular chromium-chromium sepation is 8.136(1) Å [Cr(1)···Cr(1a)].

$[\{Cr(bipy)(CN)_4\}_2Mn(H_2O)_4]\cdot 4H_2O$ (2): The structure of **2** is made up of centrosymmetric neutral trinuclear units of formula $[\{Cr(bipy)(CN)_4\}_2Mn(H_2O)_4]$ where the $[Cr(bipy)(CN)_4]^-$ entity acts as a monodentate ligand through one of its four cyanide groups toward a central $[Mn(H_2O)_4]^{2+}$ motif (Figure 2). Four water molecules of crystallization

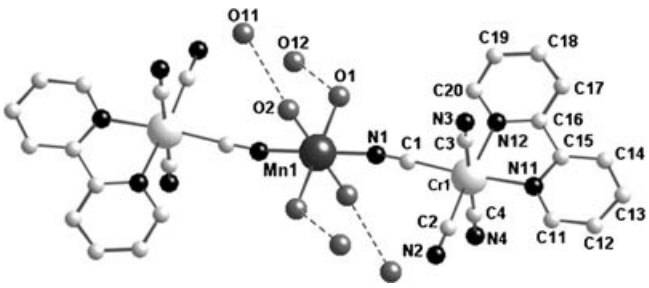

Figure 2. Perspective drawing of the centrosymmetric trinuclear unit of **2** along with the atom numbering. Hydrogen bonds between the coordinated and crystallization water molecules are illustrated by dotted lines.

contribute to the stabilization of the structure through hydrogen bonds involving the coordinated and lattice water molecules and one of the three terminal cyanide ligands [2.660(9), 2.794(11) and 2.782(8) Å for O(1)···O(12), O(2)···O(11) and O(1)···N(3b), respectively] (Figure 3).

As in **1**, each chromium atom is coordinated by two bipy nitrogen atoms and four cyanide carbon atoms, in a distorted octahedral geometry. The values of the Cr–N(bipy) bonds and that of the angle subtended at the chromium

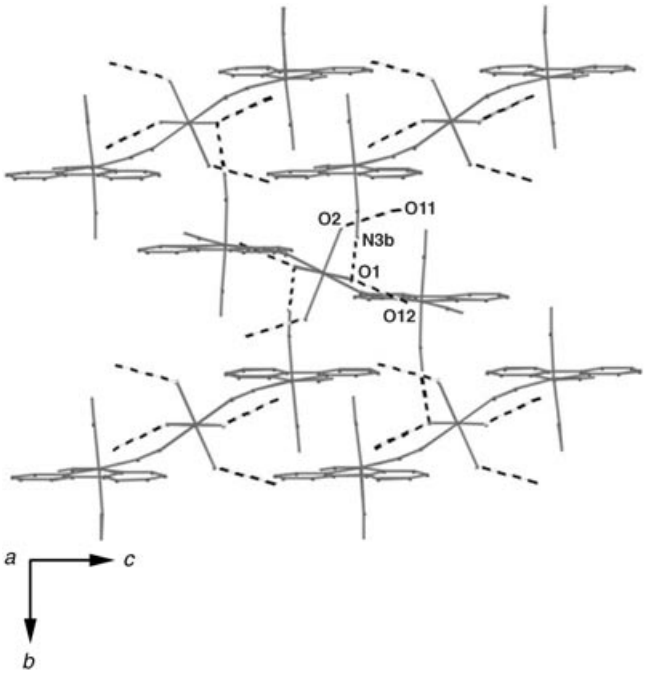

Figure 3. A view of the hydrogen bonding pattern in **2**.

atom by the chelating bipy are very close to those found in **1**. The values of the two Cr–C(cyano) bonds coordinated in *trans* positions to each other are slightly longer than those in the *cis*-coordinated ones, as observed in the parent trinuclear complexes of formula $[\{Fe(bipy)(CN)_4\}_2M(H_2O)_4]\cdot 4H_2O$ [M = Mn^{II} and Zn^{II}].[16b] The Cr-C-N angles for the terminal cyanide groups deviate somewhat from 180° [177.9(6)–175.3(7)°] whereas those for the bridging cyanide, Cr-C-N [170.7(7)°] and Mn-N-C [168.9(6)°] exhibit a greater bending. The manganese atom is six-coordinated with two cyanide-nitrogen atoms in *trans* position and four water molecules, building a distorted MnN_2O_4 octahedral surrounding. The presence of three peaks in the CN stretching region of the infrared spectrum of **2** is in agreement with the occurrence of bridging (2157(m) cm^{-1}) and terminal (2138(m) and 2131(w) cm^{-1}) cyanide ligands.

The five-membered chelate Cr(1)-N(11)-C(15)-C(16)-N(12) is practically planar [the largest deviation from the mean plane is 0.038 Å for C(11)]. Although the shortest intermolecular bipy–bipy contacts are 3.356 (cycle 1 with cycle 2c; cycle 1 = N(11)/C(15), cycle 2 = N(12)/C(20) and c = $2-x$, $1-y$, $1-z$], 3.385 [cycle 1 with cycle 2d; d = x, $^3/_2-y$, $-^1/_2+z$] and 3.435 Å [cycle 1 with cycle 1e; e = $2-x$, $1-y$, $-z$] (Figure S3), a weak overlap between the bipy mean planes occurs because of their relative large slipping.

The intramolecular Cr(1)···Mn(1) separation across bridging cyanide in **2** is 5.364(1) Å, a value which is somewhat greater than those observed for the Fe^{III}···Mn^{II} pair through single cyano bridges in the trinuclear $[\{Fe(bipy)(CN)_4\}_2Mn(H_2O)_4]\cdot 4H_2O$ [5.126(1) Å][16b] and tetranuclear $(\mu\text{-bipym})[Mn(H_2O)_3\{Fe(bipy)(CN)_4\}]_2[Fe(bipy)(CN)_4]_2\cdot 12H_2O$ (bipym = 2,2′-bipyrimidine) [5.092(4) Å][16c] compounds. This shortening of the metal–metal separation in the last two compounds is mainly due to the occurrence of low-spin iron(III) in them. The value of the intramolecular chromium–chromium separation [10.728(2) Å for Cr(1)···Cr(1a)] is longer than the shortest intermolecular metal–metal distances [6.899(1), 6.463(1) and 9.013(1) Å for Cr(1)···Cr(1d), Cr(1)···Mn(1f) and Mn(1)···Mn(1f), respectively; f = $1-x$, $^1/_2+y$, $^1/_2-z$].

$[\{Cr(bipy)(CN)_4\}_2Mn(H_2O)_2]$ (3): The structure of **3** consists of neutral cyanide-bridged crossed Cr^{III}–Mn^{II} zigzag chains of formula $[\{Cr(bipy)(CN)_4\}_2Mn(H_2O)_2]$ which are liked by hydrogen bonds and van der Waals forces. Within each chain, the $[Cr(bipy)(CN)_4]^-$ unit acts as a bis-monodentate bridging ligand towards two *trans*-diaquamanganese(II) entities through two of its four cyanide groups in *cis* positions affording bimetallic chains which run parallel to the *a* axis (Figure 4). This structural type has been described as a 4,2-ribbon-like chain[4] and it is isostructural with the bimetallic one-dimensional compounds $[\{Fe^{III}(L)(CN)_4\}_2M^{II}(H_2O)_2]\cdot 4H_2O$ [L = phen (M = Co, Mn and Zn) and bipy (M = Co)].[16a,25] Hydrogen bonds between the coordinated water molecules and one of the terminal cyanide nitrogen atoms [2.752(7) Å for O(1)···N(2f) and O(1e)···N(2); f = $^1/_2-x$, $-^1/_2+y$, $^3/_2-z$ and e = $^1/_2-x$, $^1/_2+y$, $^3/_2-z$] (Figure S4) connect the chains of **1** leading to a three dimensional structure.

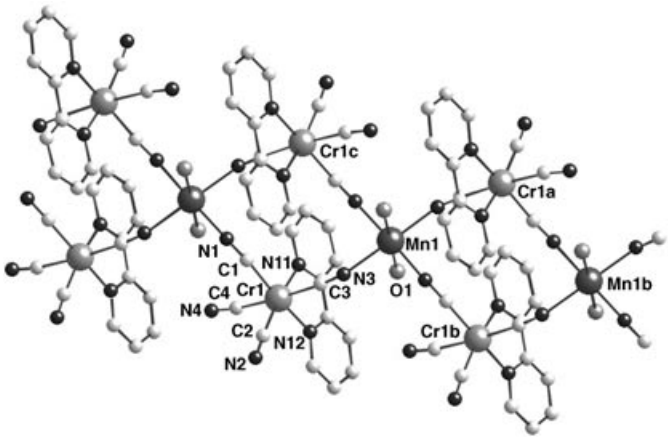

Figure 4. Perspective view of a frament of the crossed zigzag chain of **3** running parallel to the *a* axis.

The chromium and manganese atoms in **3** are six-coordinate: two nitrogen atoms from bipy and four cyanide carbon atoms around the chromium center, and two water molecules in *trans* positions and four cyanide nitrogen atoms around the cobalt center build distorted octahedral geometries. The bond lengths and angles around the chromium atom in the $[Cr(bipy)(CN)_4]^-$ unit of **3** agree with those observed for this unit in **1** and **2**. The Cr(1)-C-N angle for the bridging cyanide[169.6(5)°] exhibits a greater bending than those of the terminal cyanides [174.9(5)–172.3(5)°], as in **2**. The values of the Mn–O_{water} [2.179(4) Å] and Mn–N(cyanide) [2.245(5) and 2.222(5) Å] bond lengths in **3** are very close to those observed for the manganese(II) ion in the trinuclear complexes **2** and $[\{Fe^{III}(bipy)(CN)_4\}_2Mn^{II}$-

$(H_2O)_4]\cdot 4H_2O$ [MnN_2O_4 chromophore][16b] and in the bimetallic chain $[\{Fe^{III}(phen)(CN)_4\}_2Mn^{II}(H_2O)_2]\cdot 4H_2O$ [MnN_4O_2 chomophore].[16a] The departure from the strict linearity of the Mn(1)-N(1)-C(1) [140.5(4)°] and Mn(1)-N(3b)-C(3b) [139.6(5)°] bond angles in **3** is the largest one observed for this motif [values to be compared with 168.9(6), 159.5(6) and 161.2(3)° in **2**, $[\{Fe^{III}(bipy)(CN)_4\}_2Mn^{II}(H_2O)_4]\cdot 4H_2O$ and $[\{Fe^{III}(phen)(CN)_4\}_2Mn^{II}(H_2O)_2]\cdot 4H_2O$, respectively]. The C–N bond lengths for terminal and bridging cyanide ligands [1.146(7)–1.132(7) Å] compare well with those observed in **2** [1.160(9)–1.142(9) Å]. The IR spectrum of **3** provides spectral evidence of the occurrence of bridging (2143(m) cm^{-1}) and terminal (2130(w) cm^{-1}) cyanide ligands.

The five-membered chelate Cr(1)-N(11)-C(15)-C(16)-N(12) is almost planar [the largest deviation from the mean plane is 0.047 Å for C(19)]. Although the shortest intermolecular bipy–bipy contacts are about 3.60 Å, the large slipping of the bipy planes prcludes any significant π–π interaction (Figure S5). The values of the intrachain chromium–manganese separation through bridging cyanide are 5.021(1) [Cr(1)···Mn(1)] and 5.029(1) Å [Cr(1)···Mn(b)], values which are somewhat shorter than that observed in **2** due to the greater bending of the Mn-N-C motif in **3**. Other relevant intrachain metal–metal distances are 6.220(2) [Cr(1)···Cr(1c)] and 7.894(4) Å [Mn(1)···Mn(1b) and Cr(1)···Cr(1b)]. The shortest interchain metal–metal separations are 6.974(1) [Cr(1)···Mn(1e)], 8.173(2) [Cr(1)···Cr(1d)] and 10.449(2) Å [Mn(1)···Mn(1g); $g = {}^1/_2-x, -{}^1/_2+y, {}^1/_2-z$].

$[\{Cr(bipy)(CN)_4\}_2Mn(H_2O)]\cdot H_2O\cdot CH_3CN$ (4): The structure of complex **4** is made up of one-dimensional $[\{Cr(bipy)(CN)_4\}_2Mn(H_2O)]$ units running parallel to the *b* axis and uncoordinated water and acetonitrile molecules. The crystallographically independent unit contains two types of chromium atoms [Cr(1) and Cr(2)] and one manganese atom [Mn(1)] (Figure 5) the latter being connected to five chromium atoms through single cyanide bridges. The uncoordinated water molecule [O(2w)] forms hydrogen bonds with the coordinated one [O(1w)] and a nitrogen atom [N(8)] of one of the terminal cyanide ligands [2.507(8) and 2.958(8) Å for O(2w)···O(1w) and O(2w)···N(8), respectively]. The $[\{Cr(bipy)(CN)_4\}_2Mn(H_2O)]$ motif builds a corrugated ladder-like chain with regular alternating Cr(1) and Mn(1) atoms along the edges, each rung being defined by a chromium–manganese pair (Figure 6). In addition, each pair of adjacent manganese atoms is connected through another chromium atom [Cr(2)]. The metal atoms are linked each other by single cyano groups. The structure of **4** can be viewed as the result of the condensation of two parallel chains of **3** shifted by *b*/2 after loss of one of the two coordinated water molecules of the manganese atom of each chain and its position being filled by a cyanide nitrogen of a terminal cyanide of the adjacent chain. Compound **4** is isostructural with the compounds of formula $[\{Fe^{III}(bipy)(CN)_4\}_2M^{II}(H_2O)]\cdot {}^1/_2 H_2O\cdot CH_3CN$ [M = Co and Mn] where low-spin iron(III) is present instead of chromium(III).[27]

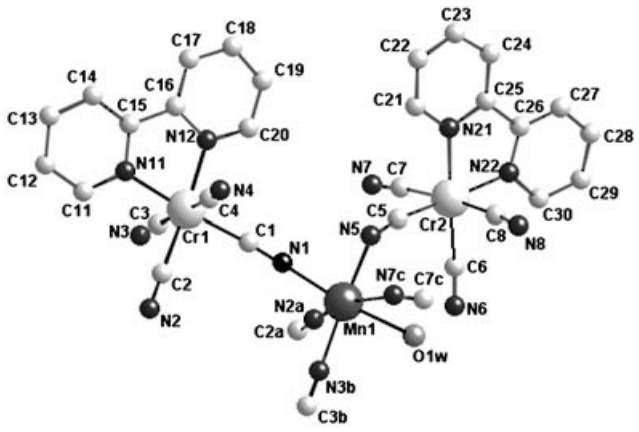

Figure 5. Perspective view of the crystallographically independent unit of **4** along with the atom numbering. Hydrogen bonds involving the water molecules and one cyanide-nitrogen atom are also shown.

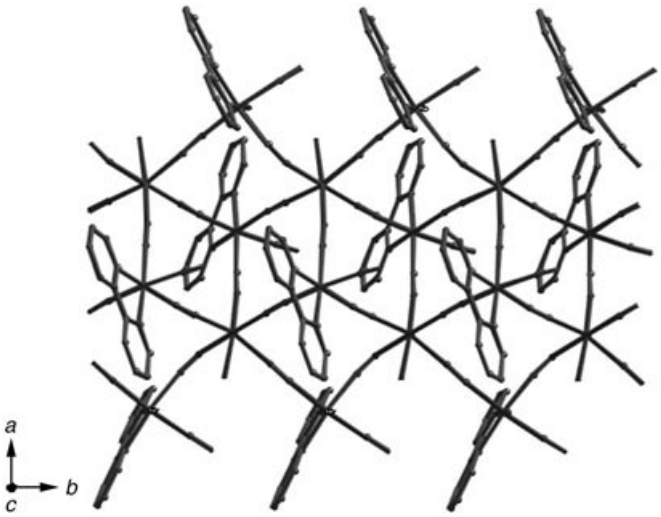

Figure 6. A view of a fragment of the double chain structure of **4** along the *b* axis. The crystallization water molecule and the hydrogen atoms have been omitted for clarity.

The two crystallographically independent chromium atoms [Cr(1) and Cr(2)] exhibit the same distorted octahedral CrN_2C_4 surrounding already observed in the structures of **1**–**3**. The difference between the $[Cr(1)(bipy)(CN)_4]^-$ and $[Cr(2)(bipy)(CN)_4]^-$ units is that the former acts as a trismonodentate ligand toward the manganese atom through three (*fac* position) of its four cyanide groups, only one of its four cyanide ligands being terminal, whereas the latter adopts a bismonodentate coordination mode through two cyanide ligands in *cis* position. The Cr-C-N angles for both terminal [175.7(3)° at Cr(1) and 176.5(3) and 176.9(3)° at Cr(2)] and bridging [176.5(3), 176.0(3) and 173.9(3)° at Cr(1) and 171.0(3) and 175.1(3)° at Cr(2)] cyanide groups are somewhat bent. The manganese atom is six-coordinate with five cyanide nitrogen atoms and a water molecule forming a distorted MnN_5O octahedral chromophore. The deviations from the mean basal plane around the manganese atom are ±0.13 Å, the metal atom being shifted by 0.22 Å from this mean plane toward the apical N(1) atom. The C–N bond lengths for terminal and bridging cyanide ligands [1.136(5)–

1.148(5) Å] are in agreement with those observed in **3**. Spectroscopic evidence for the occurrence of bridging and terminal cyanide ligands in **4** is provided by the presence of cyanide stretching vibrations at 2159(m) (bridging cyanide) and 2134 cm^{-1} (terminal cyanide) in its IR spectrum.

The large separation between the parallel and quasi eclipsed bipy ligands of each double chain along the *b* axis precludes any significant π–π intrachain interaction. Although interchain bipy–bipy contacts occur (the separation between the mean planes of neighbouring bipy ligands is 3.80 Å), the large slipping between the aromatic heterocycles minimizes them (Figure S6). The values of the dihedral angle between adjacent mean planes of the corrugated

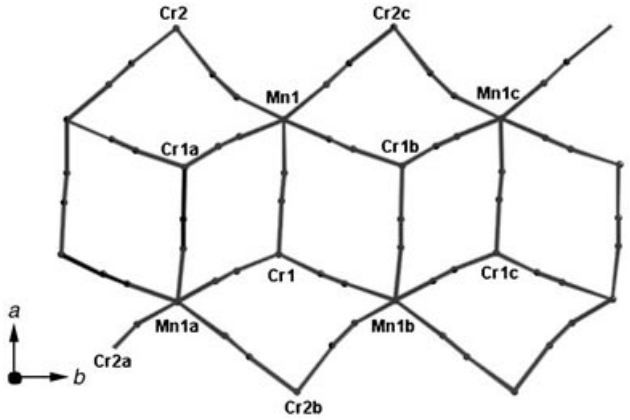

Figure 7. A schematic view of a fragment of a double chain of **4** where only the metal atoms and the cyanide bridges (full lines) are included. Symmetry codes: a = $^3/_2-x$, $-^1/_2+y$, $^1/_2-z$; b = $^3/_2-x$, $^1/_2+y$, $^1/_2-z$; c = x, $1+y$, z.

ladder-like motif (Figure 7) are 80 [dihedral angle between Cr(1)-Mn(1)-Cr(1a)-Mn(1a) and Cr(1)-Mn(1)-Cr(1b)-Mn(1b)], 83 [Cr(1b)-Mn(1)-Cr(2c)-Mn(1c) and Cr(1)-Mn(1)-Cr(1a)-Mn(1a)] and 74° [Cr(1b)-Mn(1)-Cr(2c)-Mn(1c) and Cr(1b)-Mn(1)-Cr(2c)-Mn(1c)]. The values of the chromium–manganese distances across bridging cyanide are 5.406(2) [Cr(1)···Mn(1)], 5.418(1) [Cr(1)···Mn(1a)], 5.373(1) [Cr(1)···Mn(1b)], 5.108(1) [Cr(2)···Mn(1)] and 5.406(1) Å [Cr(2c)···Mn(1)]. The shortest intermolecular metal-metal separations are 8.861(3) [Mn(1)···Cr(1d); d = $x+^1/_2$, $-y+^3/_2$, $z+^1/_2$] and 9.015(2) Å [Mn(1)···Cr(2e); e = $-x+2$, $-y+1$, $-z$].

Magnetic properties

Compound 1: The magnetic properties of complex **1** in the form of the $\chi_M T$ product against T plot [χ_M being the magnetic susceptibility per mol of Cr^{III}] are shown in Figure S7. At room temperature, $\chi_M T$ for **1** is 1.84 $cm^3 mol^{-1} K$, a value which is as expected for a magnetically isolated spin quartet. It remains constant upon cooling and only decreases slightly at very low temperatures reaching a value of 1.68 $cm^3 mol^{-1} K$ at 1.9 K. No susceptibility maximum was observed in the temperature range investigated. The slight decrease of $\chi_M T$ at lower temperatures may be attributed to the zero fied splitting (D) of the chromium(III) ion, to weak antiferromagnetic intermolecular interactions or to both factors simultaneously. Having in mind the mononuclear nature of the paramagnetic mononuclear unit in **1**, we have analysed its magnetic data through the Hamiltonian given by Equation (1) (case of an axial zero field splitting and S = $^3/_2$):[34]

$$\hat{H} = D[\hat{S}_z^2 - {}^1/_3 S(S+1)] \quad (1)$$

The least-squares fit of the $\chi_M T$ data of **1** through the expression derived from Equation (1) leads to the following set of parameters: $|D| = 0.8\ cm^{-1}$, $g = 1.98$ and $R = 1.1 \times 10^{-5}$ (R is the agreement factor defined as $\Sigma_i[(\chi_M T)_{obs}(i) - (\chi_M T)_{calcd}(i)]^2/\Sigma_i[(\chi_M T)_{obs}(i)]^2$). The computed curve matches well the experimental data in the whole temperature range. As the Brillouin function for a magnetically isolated spin quartet with $g = 1.98$ reproduces well the magnetization versus H data of **1** at 2.0 K (see inset of Figure S7), it is clear that we are dealing with a magnetically isolated spin quartet with a very weak magnetic anisotropy. Consequently, the magnetic coupling between the spins of the Cr(1) and Cr(1a) atoms through the Cr(1)-CN···water···NC-Cr(1a) pathway (see Figure S1) has to be very weak, if any.

Compound 2: The magnetic properties of **2** (together with those of **3**) in the form of both $\chi_M T$ and χ_M versus T plots [χ_M is the magnetic susceptibility per mol of $Cr^{III}_2Mn^{II}$ trinuclear unit in **2** and **3**] are shown in Figures 8 and 9, respectively. Let us focus first on the magnetic properties of complex **2**. $\chi_M T$ of **2** at 295 K is 7.90 $cm^3 mol^{-1}$, a value which is somewhat below that calculated for two magnetically isolated spin quartets [Cr^{III}] and one spin sextet [Mn^{II}] (8.13 $cm^3 mol^{-1} K$ with $g = 2.0$). This value continuously decreases upon cooling (Figure 8) and it exhibits a plateau with $\chi_M T = 0.36\ cm^3 mol^{-1} K$ at $T \leq 5$ K (see inset of Figure 8). The χ_M versus T plot of **2** continuously increases upon cooling, it exhibits a maximum at 25 K with $\chi_M =$

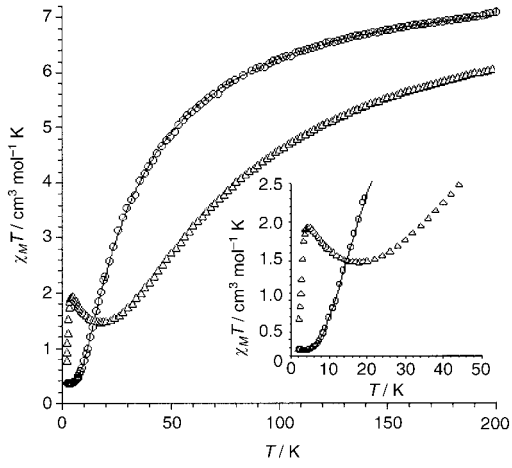

Figure 8. Temperature dependence of the $\chi_M T$ product of **2** (○) and **3** (△). The inset is an expanded view of the low temperature region. The solid line in **3** is the best-fit curve by the analytical expression derived through Equation (2) (see text).

$0.12\ cm^3 mol^{-1}$ (Figure 9), then a minimum at 7.0 K ($\chi_M = 0.068\ cm^3 mol^{-1}$) and sharply increases at lower temperatures. These features are indicative of a significant intramolecular antiferromagnetic coupling between Cr^{III} and Mn^{II}, the plateau of $\chi_M T$ at very low temperatures being due to the full population of the low-lying spin doublet (antiferromagnetic interaction between the central spin sextet of the Mn^{II} and the two peripheral spin quartets of the two Cr^{III} ions]. This ground spin doublet accounts for the Curie tail of the χ_M versus T plot of **2** at very low temperatures (Figure 9). In order to fit the magnetic data of the trinuclear compound **2**, we have used the analytical expresion derived from the Hamiltonian given in Equation (2):

$$\hat{H} = -J[\hat{S}_{Cr(1)} \cdot \hat{S}_{Mn(1)} + \hat{S}_{Cr(1a)} \cdot \hat{S}_{Mn(1)}] \quad (2)$$

where J is the magnetic coupling parameter between the central manganese(II) ion and each peripheral chromium(III) ion. The zero-field splitting effects and the magnetic coupling (j) between the peripheral chromium(III) ions (intramolecular chromium-chromium separation larger than 10.7 Å) were not considered. A least-squares fit leads to the following set of parameters: $J = -6.2\ cm^{-1}$, $g = 1.98$ and $R = 1.1 \times 10^{-5}$ (R is the agreement factor defined as $\Sigma_i[(\chi_M)_{obs}(i) - (\chi_M)_{calcd}(i)]^2/\Sigma_i[(\chi_M)_{obs}(i)]^2$). The computed curve matches very well the magnetic data in the whole temperature range.

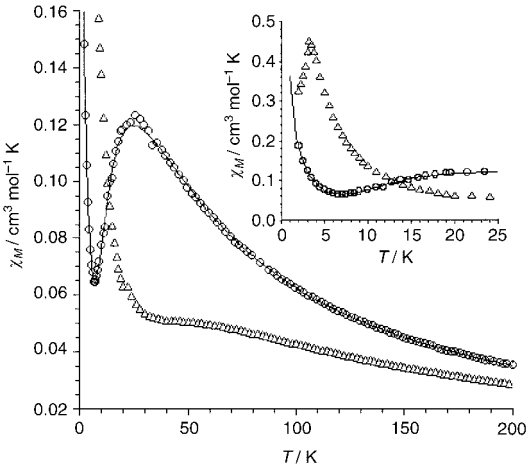

Figure 9. Temperature dependence of χ_M for **2** (○) and **3** (△). The inset shows the low temperature region but covering a larger range of values of χ_M. The solid line in **2** is the best-fit curve through Equation (2) (see text).

As far as the magnitude of the antiferromagnetic interaction between Cr^{III} and Mn^{II} in **2** is concerned ($J = -6.2\ cm^{-1}$), its value compares well with those reported for this couple in two different heptanuclear complexes $[Cr^{III}\{CN\text{-}Mn^{II}(tetren)_6\}]^{9+}$ with tetren = tetraethylenepentamine (-10.8 and $-7.2\ cm^{-1}$).[5a] Structural differences (nature of the donor atoms around the manganese atom, degree of bending at the Cr-C-N-Mn bridging, etc.) are most likely the main factors that explain the slight variation of $-J$ in this set of compounds.[35] Concerning the sign of the magnetic coupling in **2**, in the light of the the electronic configurations of the interacting metal ions $[t_{2g}^3 e_g^0$ and $t_{2g}^3 e_g^2$ for octahedral Cr^{III} and Mn^{II} centres, respectively], one can see that antiferro- $[t_{2g}(Cr)-t_{2g}(Mn)]$ and ferromagnetic $[t_{2g}(Cr)-e_g(Mn)]$ contributions are involved, the former ones being dominant in the present case.[36] This point will be discussed in more detail by means of theoretical calculations (see below).

Compound 3: The magnetic properties of **3** (Figure 8) reveal the occurrence of an overall intrachain antiferromagnetic coupling between Cr^{III} and Mn^{II} ions, the $\chi_M T$ versus T plot for **3** being below that of **2** for $T > 13$ K. $\chi_M T$ at 295 K for **3** is $7.0\ cm^3 mol^{-1} K$, a value which is well below that calculated for two magnetically non-interacting spin quartets and one spin sextet ($8.13\ cm^3 mol^{-1} K$ with $g = 2.0$). Upon cooling, $\chi_M T$ for **3** decreases faster than in **2**, attains a minimum at 20 K, then smoothly increases to reach a maximum at 4.6 K and further decreases to $0.75\ cm^3 mol^{-1} K$ at 1.9 K (see inset of Figure 8). The magnetic susceptibility of **3** (Figure 9) increases first when cooling from room temperature, exhibits a shoulder in the temperature range 60–35 K, then increases to reach a maximum at 3.5 K and further decreases to $\chi_M = 0.32\ cm^3 mol^{-1}$ at 1.9 K (see inset of Figure 9). No signal was observed for the ac magnetic susceptibility measurements of **3** at $T < 10$ K. These magnetic features can be interpreted as follows: the intrachain antiferromagnetic coupling between Cr^{III} and Mn^{II} through the two single cyanide bridges leads to a ferrimagnetic chain which accounts for the decrease of $\chi_M T$ in the high temperature range and the occurrence of a minimum of $\chi_M T$ at low temperaures. Weak interchain antiferromagnetic interactions cause the maximum of magnetic suceptibility at 3.5 K (under an applied magnetic field of 50 Oe). This maximum disappears for $H >$ 3000 Oe and thus the magnetic behaviour of compound **3** is that expected for a metamagnet. In fact, this interpretation is supported by the magnetization plot per $Cr_2^{III}Mn^{II}$ unit of **3** at 2.0 K (Figure 10). The saturation value of the magnetization $M_S = 0.98$ BM at 5 T is as expected for a low-lying spin doublet with $g = 1.98$ ($S = 2S_{Cr} - S_{Mn} = {}^6/_2 - {}^5/_2 = {}^1/_2$). The sigmoidal shape of the M versus H plot (see inset of Figure 10) is the signature of the metamagnetic behaviour of **3**.[37] The value of the critical field $H_c = 3000$ Oe (the inflexion point in the inset of Figure 10) allows the estimation of a value for the interchain magnetic interaction of about $0.3\ cm^{-1}$. The lack of a theoretical model to analyze the magnetic data of **3**, precludes the determination of the values of the two intrachain magnetic interactions between Cr^{III} and Mn^{II}. It is clear that the magnetic coupling obtained in **2** could be taken as a rough estimation (everything being equal). Anyway, we tried to evaluate the intrachain magnetic interactions in **3** through DFT type calculations and Monte Carlo simulations (see below).

Compound 4 under high magnetic fields: The magnetic properties of **4** in the form of $\chi_M T$ and χ_M versus T plots [χ_M is the magnetic susceptibility per $Cr_2^{III}Mn^{II}$ unit] at three different magnetic fields are shown in Figure 11. Let us focus first on the magnetic plot at $H = 1$ T. This plot follows quite well that of the related chain **3**. $\chi_M T$ for **4** at 300 K is $6.20\ cm^3 mol^{-1} K$, a value which is somewhat below that of **3**

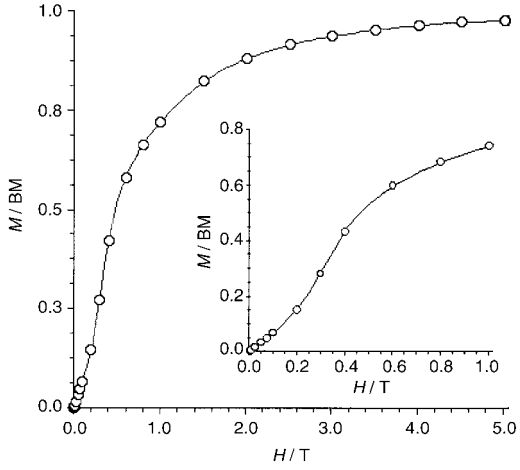

Figure 10. Magnetization versus H plot for **3** at 2.0 K. The inset shows the low field region. The solid line is an eye-guide.

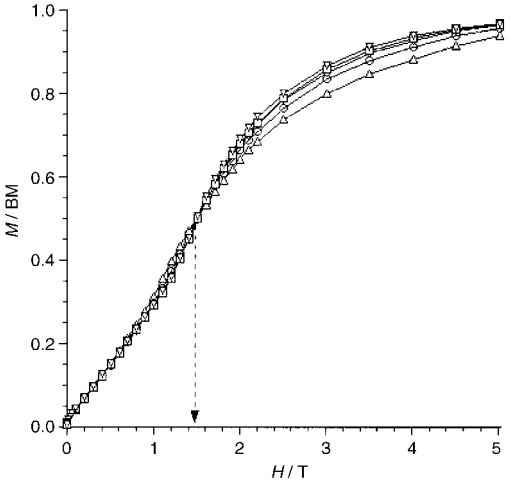

Figure 12. Isotherms ($2 \leq T \leq 8$) of the magnetisation versus H plot for **4**. 8 K (△), 6 K (○), 4 K (◇), 3 K (□), 2 K (▽).

($7.0\ cm^3 mol^{-1}$) suggesting that a stronger antiferromagnetic coupling occurs in **4**. $\chi_M T$ continuously decreases when cooling, reaches a minimum at 26 K, then smoothly increases to reach a maximum at 5.1 K and further decreases to $0.65\ cm^3 mol^{-1} K$ at 1.9 K. The corresponding magnetic susceptibility plot (see bottom curve in the inset of Figure 11)

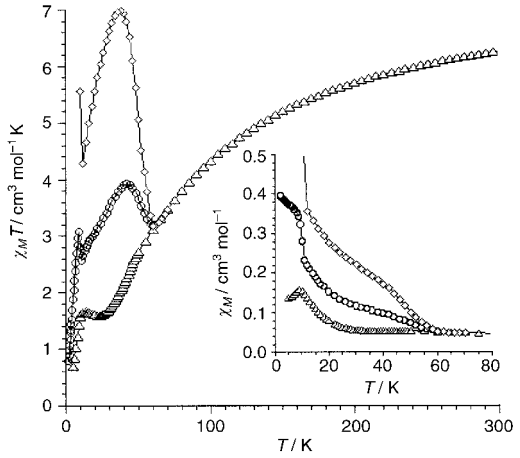

Figure 11. Temperature dependence of the $\chi_M T$ product of **4** (△) under an applied magnetic field of 1 T (△), 250 Oe (○), and 50 Oe (◇). The inset shows the thermal dependence of the magnetic susceptibility at $T \leq$ 75 K.

exhibits a maximum at 9.5 K [a value somewhat greater than that observed for **3** (3.5 K)] which disappears for $H >$ 1.5 T. The magnetization versus H plot for **4** in the temperature range 8.0–2.0 K (Figure 12) tends to quasi-saturation value of 0.97 BM and the curves have a sigmoidal shape, with a critical field of about 1.5 T (compared with 0.3 T in **3**). These magnetic features of **4** are thus like those of **3**, the higher value of the critical field in **4** respect to that in **3** being in agreement with the somewhat greater temperature of the susceptibility maximum for **4**. In conclusion, **3** and **4** are ferrimagnetic chains with interchain antiferromagnetic interactions which can be broken by the applied field leading to metamagnetism. The interchain magnetic interactions are larger for **4** as demonstrated by its larger H_c value (1.5 T in **4** versus 0.3 T in **3**).

Compound 4 under low magnetic fields: As shown in Figure 11, the low temperature magnetic plots are strongly modified when lowering the applied field. A minimum of $\chi_M T$ appears at $\approx$60 K and a pronounced maximum of $\chi_M T$ appears at $\approx$30 K under applied fields of 250 and 50 Oe and a further increase of $\chi_M T$ is observed at very low temperatures when $H = 50$ Oe. The susceptibility maximum observed under $H = 1$ T disappears when lowering the field (see inset of Figure 11) and magnetic ordering occurs as indicated by the presence of a frequency-independent maximum of the imaginary component of the ac signal (Figure S8). Because of the reproducibility of this magnetic behaviour of **4** (crushed crystals of two different batches of this compound were investigated), the presence of magnetic impurities accounting for this strong field dependence was discarded.

This curious behaviour may be due to a situation of spin canting within the double chain which can arise from antisymmetric exchange.[38] The lack of inversion center within each double chain of **4** supports this assumption. The antisymmetric exchange term, tends to align spins perpendicular to each other and competes with the spin-(anti)parallel alignment imposed by the isotropic (anti)ferromagnetic exchange. The existence of correlation of spin canting within the chain causes the increase of $\chi_M T$ below 60 K under low applied magnetic fields (250 and 50 Oe in Figure 11). High fields (such as 1 T) overcome the antisymmetric exchange and mask the effect of spin canting.[38c,d] The decrease of $\chi_M T$ below 30 K is due to the interchain magnetic interactions which lead to an antiferromagnetic ordering. This antiferromagnetic interaction can be evaluated from the magnetization plot (Figure 12) and it is about $-1.5\ cm^{-1}$. Finally, as commonly occurs when the antisymmetric exchange is operative, a structure of spin canting instead of a pure antiferromagnetic one is obtained. This three-dimensional ordering of canted spins appears below 10 K, as indicated by

the fast increase of susceptibility below 10 K. Ac measurements (see Figure S8) show this magnetic ordering near 10 K. As indicated above for **3**, there is no model to analyze the magnetic properties of **4**. In order to substantiate our interpretation of the magnetic properties and to get an estimation of the values of the exchange coupling, we carried out DFT type calculations and Monte Carlo simulations also on this system (see below).

Analysis of the exchange pathways in 3 and 4: Local quartet [chromium(III)] and sextet [manganese(II)] spins interact magnetically through single cyanide bridges in the chain compounds **3** and **4**. An inspection of their structures shows that different Cr^{III}-C-N-Mn^{II} exchange pathways are present. In the case of **3**, one of the cyanide bridges [C(3)–N(3)] is perpendicular to the mean bipy plane whereas the other is coplanar with it [C(1)–N(1)]. The deviation from the strict linearity at the Cr-C-N-Mn unit in **3** is much larger at the manganese atom [average values of 171.2 and 140.0° for Cr-C-N and Mn-N-C, respectively]. In order to analyze these exchange pathways and to get an orbital picture which could account for the magnetic behaviour of **3**, we performed DFT type calculations on two mononuclear (**I** and **II**) and two heterodinuclear (**III** and **IV**) model fragments (Figure 13) whose structural parameters (bond lengths and angles) were taken from the structure of **3**. The double chain structure in **4** introduces additional intrachain exchange pathways (vertical links in Figure 7 which connect the two parallel bimetallic chains) as well as subtle structural changes [relative arrangement of the two bidentate bipy ligands and a greater linearity of the Cr-N-C-Mn units with average values of 174.5 (Cr-C-N) and 174.4° (Mn-N-C), the exception being the value of 146.8(3)° for Mn(1)-N(5)-C(5)]. Keeping in mind these features, four models (**V**–**VIII**, Figure 13) were considered to analyze the exchange pathways and their ability to mediate exchange interactions in **4**. Model **VII** corresponds to the Cr-C-N-Mn unit having the largest bending (being then closer to models **III** and **IV** for compound **3**).

The values of the calculated spin densities found for models **I** and **II** are listed in Table 6. One can see there that a non negligible amount of the spin density of the manganese(II) is delocalized on the donor atoms of the ligands through e_g-type orbitals. As far as the Cr^{III} ion is concerned, as it has no e_g-magnetic orbitals, the delocalization on the donor atoms of the ligands is practically inexistent. As previously observed by one of us in the $[Cr(CN)_6]^{3-}$ unit,[39] the Cr^{III} ion only delocalizes its spin density on the nitrogen atom of the cyanide ligand and not on the carbon one due to the non-bonding character of the singly occupied molecular orbital (SOMO) (see Figure 14a). Then, the carbon atom undergoes spin polarization effects caused by the spin densities of the neighbouring atoms. This spin polarization results in a delocalization of α-type electrons from the filled orbitals of the carbon atom toward empty orbitals of the metal ion causing a negative spin density on the carbon atom. With these results in mind [t_{2g} (Cr and Mn) and e_g (Mn) magnetic orbitals in **I** and **II**], we focused on the heterodinuclear models **III**–**VIII** that visualize the exchange pathways through the cyanide bridges within the single (**3**) and double (**4**) chains. In order to evaluate all magnetic interactions occurring in **3** and **4**, which correspond to the models **III** and **IV** (**3**) and **V**–**VIII** (**4**), the most stable configuration was determined through DFT calculations on the nonet and triplet spin states. This determination is not a simple task due to the different solutions closer in energy which are found for

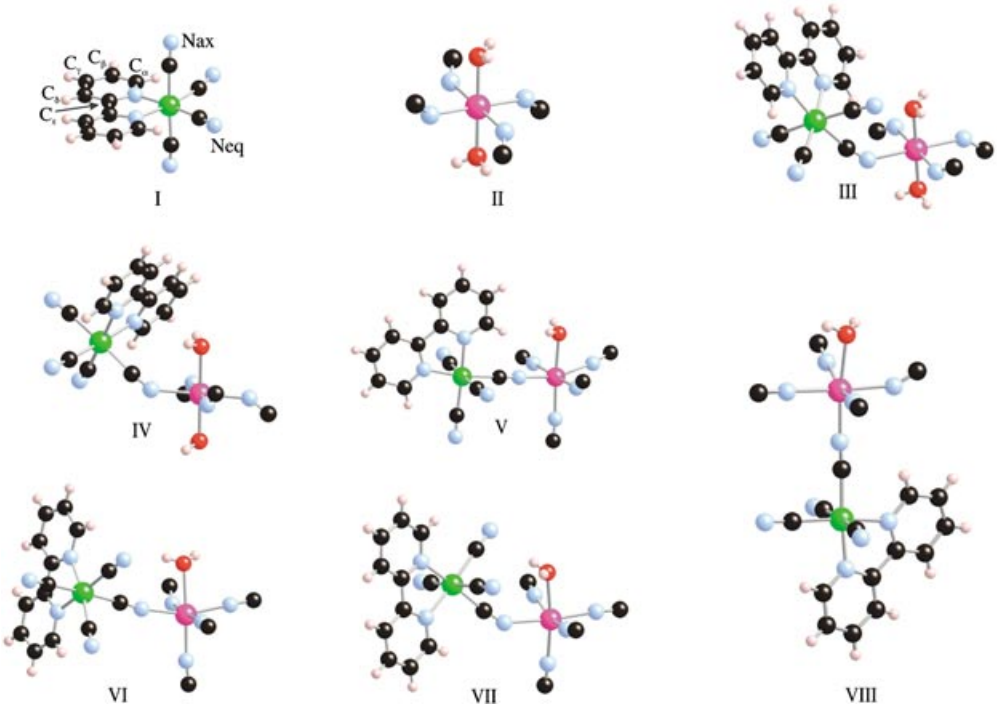

Figure 13. Mononuclear (**I** and **II**) and heterodinuclear (**III**–**VIII**) models used in the DFT calculations concerning compounds **3** and **4**.

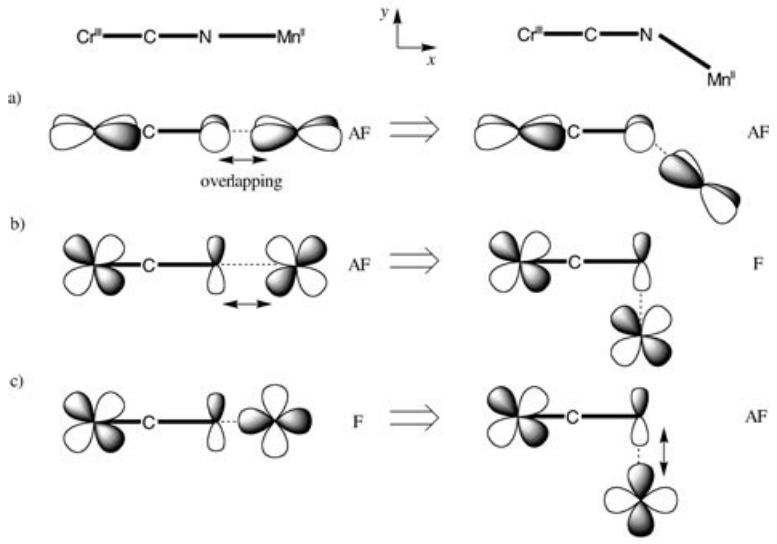

Figure 14. Most important contributions to the magnetic coupling in compounds **3** and **4** showing the influence of the deviation of the linearity of the Cr-C-N-Mn unit on them.

Table 6. Average values of the atomic spin densities in electron units found in models **I** and **II**.

	III		
Atom	Spin density	Atom	Spin density
Cr	2.964 (2.716/0.2333)[a]	Mn	4.762
$C(CN)_{eq}$	−0.095	$C(CN)_{eq}$	0.030
$C(CN)_{ax}$	−0.074	$N(CN)_{eq}$	0.013
$N(CN)_{eq}$	0.086	$O(w)_{ax}$	0.030
$N(CN)_{ax}$	0.074		
N(bipy)	−0.026		
C_α	0.027		
C_β	−0.010		
C_χ	0.023		
C_δ	−0.009		
C_ε	0.023		

[a] Values of the spin density of the t_{2g} and e_g orbitals of the Cr^{III} ion, respectively.

this type of systems. In our case, a series of solutions which corresponds roughly to the same configuration was found. However, the energy of these solutions vary a hundred or even a thousand of cm^{-1}, which is too large for an accurate determination of the magnitude of the magnetic couplings whose values do not exceed a few cm^{-1}. A deep analysis of the wave function, reveals the occurrence of slight changes which do not modify the global description of the system. However, due to the lack of ambiguity in the electronic configurations of the chromium(III) and manganese(II) ions, this problem is not too dramatic. In any case, the stability test was carried out on the wave function of the more stable solution. The computed values for the magnetic couplings of the models **III**–**VIII** are listed in Table 7. Although their respective values are clearly overestimated, their antiferromagnetic nature is in agreement with the experimental behaviour found for **3** and **4**. This problem was also observed in all models when using different basis sets for the metal and non-metal ions and in general, the changes of the basis sets do not modify strongly the values of the magnetic interactions (as shown in Table 7). The overestimation of the magnetic coupling could be due to the problems associated to the determination of the more stable wave function, as suggested by the fact that the value of the magnetic coupling for model **VIII** clearly changes when changing the basis set going from those found for **III** and **IV** to the values computed for **V**, **VI** and **VII** independently on the basis set used.

The difficulty to find the most stable solution may lie in the probable influence on the calculations by the mixing of the t_{2g} [Cr^{III} and Mn^{II}] and π^* (bipy) orbitals, which are very close in energy. In order to test this hypothesis, the bipy ligands in **III**–**VIII** were replaced by two ammonia groups. Obviously, the Fe–N(ammonia) bond lengths were also optimized (the original bond angles being kept) to reproduce the ligand field strength of the nitrogen heterocycle. The values of the magnetic coupling obtained are listed in the A series of Table 8. In the light of these values, three points deserve to be outlined: i) their sign is identical to that found previously (see Table 7); ii) the range of variation is more reduced and iii) their magnitude is much smaller and most likely, they are more reasonable from a physical point of view. When the terminal cyanide ligands from the situation A are substituted by ammonia groups (B series in Table 8), the range of variation is narrower and the values are closer to the experimental ones. In spite of the loss of the π-character of the peripheral ligands when replacing them by ammonia groups, this last modelization seems to provide a better approach to the actual values.

According to the intensity of the magnetic coupling, the results obtained through the simplest models (see Table 8) can be grouped in two blocks: one concerning the magnetic couplings of **III**, **IV** and **VII** (J values going from −20.0 to $-14.5\ cm^{-1}$) and the other with those of **V**, **VI** and **VIII** (J

Table 7. Values of the magnetic coupling obtained through DFT calculations on the models **III**–**VIII** by using differents basis sets [double-ζ (DZ) and triple-ζ (TZ)].[a,b]

	III	**IV**	**V**	**VI**	**VII**	**VIII**
DZ+DZ	−15.3	−29.8	−106.0	−91.0	−132.6	−18.1
DZ+TZ	−17.6	−32.3	−117.9	−102.4	−146.0	−103.8
TZ+TZ	−15.7	−30.2	−109.3	−91.8	−140.8	−94.8

[a] The values of the magnetic coupling are given in cm^{-1}. [b] The first and second terms in the first column refer to the basis set used for the metal ion and remaining atoms, respectively.

Table 8. Values of the magnetic coupling obtained through DFT calculations on the models **III**–**VIII** by using a triple-ζ basis set for all atoms.[a–c]

	III	IV	V	VI	VII	VIII
A	−15.3	−14.0	−1.5	−11.7	−26.8	−8.8
B	−20.0	−19.9	−8.3	−7.9	−14.5	−11.7

[a] The values of the magnetic coupling are given in cm^{-1}. [b] The bipyridine ligand (A and B series) and all the cyanide ligands except the bridging one (only in B series) were substituted by ammonia groups. [c] The Fe-N(ammonia) bond lengths were optimized in all cases.

values between −11.7 and −7.9 cm^{-1}). The first block has in common significant deviations from the linearity of the Cr-C-N-Mn unit at the manganese atom (40.4, 39.6 and 33.2° below the ideal value of 180° for the C-N-Mn motif), whereas a greater linearity occurs in the second block (values of 176.0. 169.8 and 176.5° for C-N-Mn). This is clear that a correlation exist between the value of the magnetic coupling and the degree of bending of the C-N-Mn unit, the antiferromagnetic interaction being reinforced as the bending increases. This trend is also observed within each block. This correlation can be explained on a simple orbital basis as visualized in Figure 14. Although there are fifteen different contributions to the exchange coupling constant in each Cr^{III}–Mn^{II} pair, the inappropriate orientation of some the magnetic orbitals involved allow us to discard most of them. Among the important antiferromagnetic contributions, the most relevant ones are those involving the two t_{2g} orbitals (d_{xz} and d_{xy}) of the Cr^{III} which are directed toward the bridging ligand because of the good overlap with the appropriate orbitals of the Mn^{II} [see Figure 14a, b]. The most important ferromagnetic contribution is associated to the interaction between one of the three t_{2g} chromium orbitals (d_{xy}) and one of the e_g manganese orbitals ($d_{x^2-y^2}$) [Figure 14c] (case of the strict orthogonality between the two interacting magnetic orbitals). One can see in Figure 14 how the bending of the C-N-Mn unit causes the following effects: i) the antiferromagnetic contribution via the π pathway is not modified with the bending in case a); ii) the antiferromagnetic contribution associated to the situation of strict linearity decreases as the bending increases in case b), whereas the antiferromagnetic contribution increases as the bending increases in case c). It deserves to be noted that this last antiferromagnetic contribution goes via σ ($d_{x^2-y^2}$ and p_y) and it balances the loss of antiferromagnetism in case b) (where the π pathway is involved. Therefore, the overall balance dictates an increase of the antiferromagnetic interaction as far as the bending of the C-N-Mn unit increases, in agreement with the results through DFT calculations.

Monte Carlo simulation of the magnetic properties of 3 and 4: The simulation of the magnetic properties is important for a correct analysis of the magnetic exchange coupling in polynuclear systems. For this purpose, procedures based on the exact energy matrix diagonalization are commonly used. However, the applicability of these procedures is limited by the size of the systems, in particular in the case of the extended ones. Monte Carlo methods are among the most used ones to analyze these latter systems. In a classical spin approach, the implementation of the Monte Carlo algorithms (CMC) is a quite easy task[40] Nevertheless, this approximation can be applied only to systems with large local spin values, as high-spin iron(III) or manganese(II) complexes. For other systems, the local spin moments have to be considered as quantum spins and consequently, the so-called quantum Monte Carlo (QMC) methods must be used. The main drawbacks associated to the use of the QMC methods are their complexity and time consuming. The occurrence of chromium(III) ($S_{Cr} = {}^3/_2$) in complexes **3** and **4**, leads us to use the QMC methods to simulate their magnetic properties. Among the possible QMC methods, we have chosen the decoupled Cell Monte Carlo method (DCM) which was proposed by Homma et al. and a modification of such approach from Miyazawa et al. that improves the results at low temperatures (mDCM).[41,42] These QMC methods are applied from the probability that implies a change in the m_s value (spin flip) for the site placed on the center of a cell or subsystem. This probability is evaluated by the exact diagonalization procedure applied to the mentioned subsystem. Thus, a better description of the spin correlation function is obtained for larger subsystem sizes, allowing the correct application of the method to lower temperatures. In the mDCM methods, the spin flip probability for the paramagnetic centre *i* is calculated also taking into account the neighbouring subsystems involving it. So, the spin correlation function is more correct for the same subsystem size.

In the MC methods, from the spin flip probabilities and using a metropolis algorithm, we can generate a sampling where the states more present are those having a more important contribution in the partition function. This sampling allows us to calculate the average magnetization at a given temperature. The molar magnetic susceptibility can be obtained from the fluctuations in the magnetization through Equation (6), where $\langle M \rangle$ and $\langle M^2 \rangle$ are the mean values of the magnetization and its square, and N, β and k have their usual meaning.

$$\chi_M T = N\beta^2/k\,(\langle M^2\rangle - \langle M\rangle^2) \qquad (6)$$

In all simulations, the number of MC steps for each temperature is $5\times10^6/T$ (T in K). Thus, we included more steps in the sampling at low temperatures where the correct equilibrium requires more recorded data. A ten per cent of the MC steps are employed for the thermalization of the system; thus we stocked the physical properties when the equilibrium is reached. Models of 90 and 180 sites were used for the single (**3**) and double (**4**) chain compounds, respectively. Periodic boundary conditions were introduced in all simulations. Deeper details on the MC simulations can be found in ref. [40].

We have applied the DCM and mDCM methods to a uniform 4,2-ribbon-like chain of interacting spins $S = {}^5/_2$ and ${}^3/_2$ (compound **3**). Two decompositions in small cells were used (Figure 15a). Overall, only the first shell of neighbours is

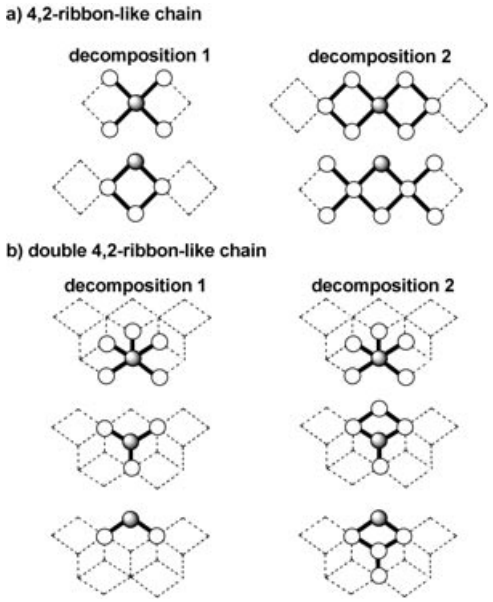

Figure 15. Decompositions in small cells of a single (a) and double (b) 4,2-ribbon-like chains which are used in the MC simulations. Bold lines refer to the global exchange topology whereas the broken ones represent the cells obtained by decomposition. The darkened circle is the central site in a given cell.

considered in the first decomposition whereas the second nearest-neighbour shell was also introduced in the second one. The simulated $\chi_M T$ versus $T/|J|$ plots for the single chain are shown in Figure 16. The three plots exhibit the shape of a ferrimagnetic system: a continuous decrease from

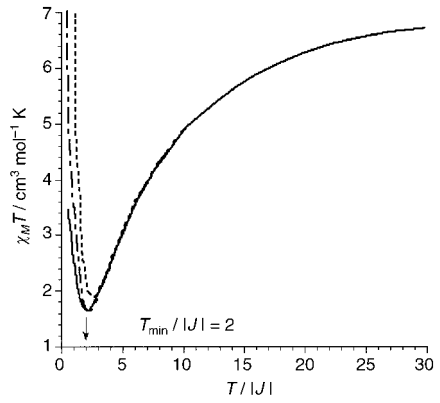

Figure 16. $\chi_M T$ versus $T/|J|$ plots for a $^5/_2$–$^3/_2$ uniform single 4,2-ribbon-like chain: DCM-1 (-----) is the method applied to decomposition 1; DCM-2 (–•–•) and mDCM-2 (——) are the methods applied to decomposition 2.

high $T/|J|$ values with a pronounced minimum at $T/|J| = 2.0$ and a sharp increase at lower $T/|J|$ values. The fact that the three plots superimpose till the minimum indicates that even the poorest simulation we performed provides a good estimation of the position of the minimum. This conclusion is very important because they can work in the case of more complex systems (double chain, **4**) where the larger subsystem size would preclude its computational treatment.

As in the case of **3**, the DCM and mDCM methods were applied to a double 4,2-ribbon-like chain of interacting spins $S = {}^5/_2$ and $^3/_2$ (compound **4**). In a first approach, only an intrachain coupling parameter was considered and not all the second shell neighbours were included for the second decomposition (Figure 15b) because of the huge size of the issued energy matrix. The simulated $\chi_M T$ versus $T/|J|$ plots for the double chain are shown in Figure 17. The coinci-

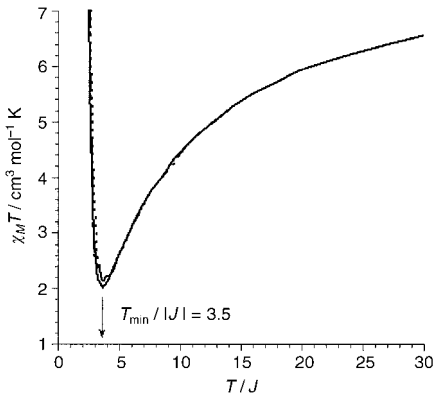

Figure 17. $\chi_M T$ versus $T/|J|$ plots for a $^5/_2$–$^3/_2$ uniform double 4,2-ribbon-like chain: DCM-1 (-----) is the method applied to decomposition 1; DCM-2 (–•–•) and mDCM-2 (——) are the methods applied to decomposition 2.

dence among the three plots is remarkable and their shape is as expected for a ferrimagnetic system. As shown in Figures 16 and 17, the single and double chain compounds have a similar magnetic behaviour. However, two important differences are observed which are due the greater number of correlation pathways in the double chain: i) the value of the $\chi_M T$ at the minimum is larger than that of the single chain and its position is shifted toward higher temperatures [$T/|J| = 3.5$ (double chain) and 2.0 (single chain)]; ii) the increase of $\chi_M T$ after the minimum is more pronounced in the double chain.

It deserves to be noted that qualitatively similar magnetic plots can be obtained under the classical spin approach for our systems. However, this approximation is unable to provide a good numerical description and this is due to the fact that $S = {}^3/_2$ for the chromium(III) ion is far from being a classical spin.

The simulated $\chi_M T$ versus $T/|J|$ plots for the single and double chains are very close to the $\chi_M T$ against T plots of **3** and **4** (at 1 T), respectively. An estimated value the intrachain exchange coupling in **3**, $J \approx -7.5\ \mathrm{cm}^{-1}$, was obtained from the QMC simulations. We have proceeded in a similar manner for complex **4** but in this case we have taken into account the presence of linear and non-linear Cr-CN-Mn exchange pathways according to the structural data. In the light of the DFT calculations, we have chosen an approximate value of 2.0 for the ratio between the exchange coupling values of the non-linear and linear exchange pathways. The estimated values are -5.2 (linear) and $-10.4\ \mathrm{cm}^{-1}$ (non-

linear). A comparison between the estimated J values of **3** and **4** and the determined one for complex **2** ($J = -6.2\ cm^{-1}$), one can see a good magneto-structural correlation in agreement with the results of the DFT calculations: the largest antiferromagnetic coupling corresponds to the higher bending of the Cr-CN-Mn unit. Finally, a rough estimation of the J value for bimetallic Cr^{III}–Mn^{II} chains with the topology of compounds **3** and **4** can be derived from the value of the $T_{min}/|J|$ which is obtained through QMC calculations.

Conclusion

In this work we show how new cyanide-bridged heterometallic Cr^{III}–Mn^{II} species [trinuclear (**2**), single (**3**) and double (**4**) chains] can be obtained by using the mononuclear complex $[Cr(bipy)(CN)_4]^-$ (**1**) as a ligand towards fully solvated manganese(II) cations in aqueous solution. The flexibility of our precursor (for instance, the bidentate bipy can be easily replaced by other chelating ligands and the number of cyanide groups depends on the denticity of these ligands) and the variety of metal ions open exciting perspectives for the metal assembling and the design of new magnetic systems. Another interesting point of the present work concerns the combined use of theoretical tools such as DFT type calculations and Monte Carlo simulations which allowed us to interpret qualitatively the magnetic properties of the single- (**3**) and double-chain (**4**) compounds. Finally, we show for the first time that QMC methods are suitable tools to analyze and to get a correct interpretation of the magnetic behaviour of these complicated magnetic systems.

Experimental Section

Materials: Chromium(III) chloride hexahydrate, manganese(II) nitrate tetrahydrate, 2,2′-bipyridine, potassium cyanide, tetraphenylphosphonium chloride and lithium perchlorate trihydrate were purchased from commercial sources and used as received. $[Cr_2(CH_3COO)_4(H_2O)_2]$ was prepared by following an experimental method already described.[43] It was kept in a desiccator over calcium(II) chloride and under anaerobic conditions. Distilled water and acetonitrile of analytical-grade quality were used as solvents. Elemental analyses (C, H, N) were performed at the Microanalytical Service of the Universidad Autónoma de Madrid. Cr/P (**1**) and Cr/Mn (**2**–**4**) molar ratios of 1:1 (**1**) and 2:1 (**2**–**4**) were determined by electron probe X-ray microanalysis at the Servicio Interdepartamental of the University of Valencia.

$PPh_4[Cr(bipy)(CN)_4]\cdot 2CH_3CN\cdot H_2O$ (1): Concentrated hydrochloric acid (3.34 mL, 20 mmol) was added to an deoxygenated aqueous suspension (20 mL) of freshly prepared chromium(II) acetate (1.88 g, 5 mmol) with continuous stirring and under argon atmosphere. The resulting blue solution became brown when mixed with solid 2,2′-bipyridine (1.56 g, 10 mmol). After this solution has been stirred for ten minutes, potassium cyanide (2.60 g, 40 mmol) dissolved in a minimum amount of dioxygen-free hot water (10 mL) was added and a brown solid was formed. It was separated by filtration in the open air and the mother liquor was poured into a concentrated aqueous solution containing PPh_4Cl (3.75 g, 10 mmol). The solution turned yellow and a crop of a yellow solid was formed on standing at room temperatures after several minutes. The solid was collected by filtration, washed with small portions of cold water and purified by recrystallisation in acetonitrile. X-ray quality crystals of **1** as well shaped yellow parallelepipeds were grown by slow evaporation of this recrystallized product in H_2O/CH_3CN (1:20) mixture. The yield is about 35%. IR (KBr pellets): ν(cyanide stretching) = 2212(w) (CH_3CN solvent molecule) and 2124(w) cm^{-1} (cyanide ligand); elemental analysis calcd (%) for $C_{42}H_{36}CrN_8OP$: C 67.13, H 4.79, N 14.91; found: C 66.91, H 4.68, N 14.79.

$[\{Cr(bipy)(CN)_4\}_2Mn(H_2O)_4]\cdot 4H_2O$ (2) and $[\{Cr(bipy)(CN)_4\}_2Mn(H_2O)_2]$ (3): Compounds **2** and **3** were obtained by using the same synthetic procedure, the only difference being that the presence of lithium perchlorate is required to get crystals of **2**. Lithium (2,2′-bipyridyl)(tetracyano)chromate(III) dihydrate (0.071 g, 0.2 mmol) [which is prepared as a yellow solid by a metathesis reaction of stoichiometric amounts of lithium perchlorate and **1** in acetonitrile] dissolved in water (10 mL) was poured into an aqueous solution (10 mL) of $Mn(NO_3)_2\cdot 4H_2O$ (0.025 g, 0.1 mmol). Yellow plates of **2** ($Mn^{2+}/[Cr(bipy)(CN)_4]^-/Li^+$ molar ratio of 1:1:40) and yellow parallelepipeds of **3** were grown from the resulting yellow solutions by slow evaporation at room temperature. The yield was almost quantitative for both compounds. IR (KBr pellets): ν(cyanide stretching) = 2157m, 2138 and 2131w (**2**) and 2143m and 2130w cm^{-1} (**3**); elemental analysis calcd (%) for $C_{28}H_{32}Cr_2MnN_{12}O_8$ (**2**): C 40.85, H 3.89, N 20.41; found: C 40.67, H 3.75, N 20.33; elemental analysis calcd (%) for $C_{28}H_{20}Cr_2MnN_{12}O_2$ (**3**): C 47.02, H 2.80, N 23.49; found: C 46.91, H 2.74, N 23.33.

$[\{Cr(bipy)(CN)_4\}_2Mn(H_2O)]\cdot H_2O\cdot CH_3CN$ (4): X-ray quality crystals of **4** were grown in a H_2O/CH_3CN (10:90 v/v) mixture by slow diffusion in an H-shaped tube of solutions of **1** (0.15 g, 0.2 mmol) at one arm and of $Mn(NO_3)_2\cdot 4H_2O$ (0.025 g, 0.1 mmol) at the other one. Yellow prisms of **4** were formed on standing at room temperature after two three weeks·The yield is about 40%. IR (KBr pellets): ν(cyanide stretching) = 2256w (CH_3CN solvent molecule) and 2159m and 2134w cm^{-1} (cyanide ligand); elemental analysis calcd (%) for $C_{30}H_{23}Cr_2MnN_{13}O_2$: C 47.65, H 3.04, N 24.07; found: C 47.54, H 2.93, N 23.91.

Physical characterisations: Infrared spectra (KBr pellets) were performed on a Bruker IF S55 spectrophotometer. Magnetic susceptibility measurements on polycrystalline samples of **1**–**4** were carried out with a Quantum Design SQUID magnetometer in the temperature range 1.9–290 K and under applied magnetic fields of 50 Oe to 1 T. Magnetization versus magnetic field measurements on **1**–**4** were carried out at 2.0 K in the field range 0–5 T. Alternating current susceptibility measurements on **3** and **4** were performed at low temperatures ($T = 20$ K) in the frequency range 0.1–1400 Hz and under an oscillating magnetic field of 1 Oe. Diamagnetic corrections of the constituent atoms were estimated from Pascal constants[44] as -471×10^{-6} (**1**), -454×10^{-6} (**2**), -376×10^{-6} (**3**) and $-404\times10^{-6}\ cm^3\,mol^{-1}$ (**4**).

Computational details: All theoretical calculations were carried out with the hybrid B3LYP method,[45–47] as implemented in the GAUSSIAN98 program.[48] Double- and triple-ζ quality basis sets proposed by Ahlrichs and co-workers have been used for all atoms.[49,50] The broken symmetry approach has been employed to describe the unrestricted solutions of the antiferromagnetic spin states.[51–54] The geometries of the mononuclear $[Cr(bipy)(CN)_4]$ (**I**) and $[Mn(H_2O)_2(NC)_4]$ (**II**) and heterodinuclear Cr^{III}–Mn^{II} (**III**–**VIII**) models were built from the experimental crystal structures. A quadratic convergence method was used to determine the more stable wave functions in the SCF process. The atomic spin densities were obtained from Natural Bond Orbital (NBO) analysis.[55–57]

Crystallographic studies: crystals of dimensions $0.30\times0.32\times0.40$ (**1**), $0.15\times0.40\times0.60$ (**2**), $0.30\times0.34\times0.42$ (**3**) and $0.10\times0.15\times0.30$ mm (**4**) were mounted on Enraf–Nonius CAD-4 (**1**–**3**) and Nonius KappaCCD (**4**) diffractometers and used for data collection. Diffraction data of **1**–**4** were collected at room temperature by using graphite-monochromated $Mo_{K\alpha}$ radiation [$\lambda = 0.71073$ (**1**–**3**) and 0.71069 Å (**4**)] with the $\omega,2\theta$ method. Accurate cell dimensions and orientation matrices (**1**–**3**) were obtained by least-squares refinements of 25 accurately centered reflections with $12 < \theta < 13°$ (**1**), $14 < \theta < 14.3°$ (**2**) and $12 < \theta < 12.3°$ (**3**). Indexing and unit cell refinement for **4** were based on all observed reflections of eight frames with the ϕ/χ scan technique, an exposure time of 56 s/frame and sample to detector distance of 35 mm. No significant variations were observed in the intensities of two checked reflections (**1**–**4**) during data collections. The data were corrected for Lorentz and polarization effects (**1**–**4**). Absorption corrections on **1**–**3** were applied by

using DIFABS[58] (**2**) and the Ψ scan curve (**1** and **3**). A summary of the crystallographic data and structure refinement is given in Table 1.

The structures of **1**–**4** were solved by direct methods through the SHELX-86[59] (**1**–**3**) and SHELX-97[60] (**4**) programs, this last one being included in WINGX[61] package. Subsequent refinement of the structures of **1**–**4** was carried out by Fourier recycling on F (**1**–**3**) and F^2 (**4**). The final full-matrix-least-squares refinement for **1**–**3** was done by the PC version of CRYSTALS,[62] and the function minimized was $\Sigma w(|F_o|-|F_c|)^2$, where $w = w'[1-(||F_o|-|F_c||)/6\sigma(F_o)^2]^2$ being $w'=1/\Sigma_r A_r T_r(X)$ with three coefficients for a Chebyshev series [7.02, −0.654 and 5.67 (**1**), 13.3, −3.76 and 10.9 (**2**) and 7.82, 1.21 and 6.48 (**3**)] for which $X=F_c/F_c(\max)$. In the case of **4**, the function minimized was $\Sigma w(|F_o|^2-|F_c|^2)^2$ where $w = 1/\sigma^2F_o^2 + (mP)^2 + nP]$ and $P=(F_o^2 + 2F_c^2)/3$ with $m=0.0508$ and $n=4.2121$. All non-hydrogen atoms in **1**–**4** were refined anisotropically. The hydrogen atoms of bipy (**1**–**4**) together with those of tetraphenylphosphonium and acetonitrile (**1**) were introduced in calculated positions whereas those of the water molecules were either located by means of a difference Fourier map (**1**–**3**) or not introduced (**4**). The coordinates of the hydrogen atoms were not refined, but they were allocated an overall isotropic thermal parameter. The values of the discrepancy indices R/R_w for all data were 0.1157/0.0558 (**1**), 0.1285/0.0688 (**2**), 0.0967/0.0717 (**3**) and 0.1298/0.1374 (**4**) [those listed in Table 1 correspond to the data with $I > 3\sigma(I)$ (**1**–**3**) and $I > 2\sigma(I)$ (**4**)]. The final geometrical calculations and graphical manipulations for **4** were carried out with PARST[63] and CRYSTALMAKER[64] programs.

CCDC-241 997 (**1**), -241 998 (**2**), -241 999 (**3**) and -242 066 (**4**) contain the supplementary crystallographic data for this paper. These data can be obtained free of charge via www.ccdc.can.ac.uk/conts/retrieving.html (or from the Cambridge Crystallographic Centre, 12 Union Road, Cambridge CB21EZ, UK; Fax: (+44) 1223-336033; or deposit@ccdc.cam.ac.uk).

Acknowledgement

We thank the Ministerio Español de Ciencia y Tecnología (Project BQU-2001-2928), the Consejería de Educación Cultura y Deportes del Gobierno Autónomo de Canarias (Project PI2002/175), the French CNRS and the European Union (Project QuEMolNa, MRTN-CT-2003-504880) for financial support. Two of us (L.T. and F.S.D.) acknowledge the Ministerio Español de Educación, Cultura y Deporte (L.T.) and Gobierno Autónomo de Canarias (F.S.D.) for pre-doctoral fellowships. Dr. J. Cano thanks the Ministerio Español de Ciencia y Tecnología for a Ramón y Cajal contract.

[1] K. R. Dunbar, R. A. Heintz, *Prog. Inorg. Chem.* **1997**, *45*, 283.
[2] M. Verdaguer, A. Bleuzen, V. Marvaud, J. Vaissermann, M. Seuleiman, C. Desplanches, A. Scuiller, C. Train, R. Garde, G. Gelly, C. Lomenech, I. Rosenman, P. Veillet, C. Cartier, F. Villain, *Coord. Chem. Rev.* **1999**, *190–192*, 1023.
[3] M. Ohba, H. Okawa, *Coord. Chem. Rev.* **2000**, *198*, 313.
[4] J. Cernák, M. Horendác, I. Potocnák, J. Chomic, A. Horendákova, J. Skorsepa, A. Feher, *Coord. Chem. Rev.* **2002**, *224*, 51.
[5] a) V. Marvaud, C. Decroix, A. Scuiller, C. Guyard-Duhayon, J. Vaissermann, F. Gonnet, M. Verdaguer, *Chem. Eur. J.* **2003**, *9*, 1678; b) V. Marvaud, C. Decroix, A. Scuiller, F. Tuyèras, C. Guyard-Duhayon, J. Vaissermann, J. Marrot, F. Gonnet, M. Verdaguer, *Chem. Eur. J.* **2003**, *9*, 1692.
[6] M. Pilkington, S. Decurtins, *Comprehensive Coordination Chemistry II. From Biology to Nanotechnology, Vol. 7* (Eds.: J. A. MacCleverty, T. J. Meyer), Elsevier, Amsterdam, **2004**, p. 177.
[7] a) K. K. Klausmeyer, T. B. Rauchfuss, S. R. Wilson, *Angew. Chem.* **1998**, *110*, 1808; *Angew. Chem. Int. Ed.* **1998**, *37*, 1694; b) A. M. A. Ibrahim, *Polyhedron* **1999**, *18*, 2111.
[8] D. J. Darensbourg, A. L. Phelps, *Inorg. Chim. Acta* **2004**, *357*, 1603, and references therein.
[9] a) T. Mallah, S. Thiébault, M. Verdaguer, P. Veillet, *Science* **1993**, *262*, 1554; b) S. Ferlay, T. Mallah, R. Ouahès, P. Veillet, M. Verdaguer, *Nature* **1995**, *378*, 701; c) R. Garde, F. Villain, M. Verdaguer, *J. Am. Chem. Soc.* **2002**, *124*, 10 531.
[10] a) W. R. Entley, G. S. Girolami, *Science* **1995**, *268*, 397; b) S. M. Holmes, G. S. Girolami, *J. Am. Chem. Soc.* **1999**, *121*, 5593.
[11] Ø. Hatlevik, W. E. Buschmann, J. Zhang, J. L. Manson, J. S. Miller, *Adv. Mater.* **1999**, *11*, 914.
[12] a) A. Sculiller, T. Mallah, A. Novorozkhin, J. L. Tholence, M. Verdaguer, P. Veillet, *New J. Chem.* **1996**, *20*, 1; b) T. Mallah, A. Marvilliers, E. Rivière, *Phil. Trans. R. Soc. Lond. A* **1999**, *357*, 3139; c) Z. J. Zhong, H. Seino, Y. Mizobe, M. Hidai, A. Fujishima, S. Ohkosi, K. Hashimoto, *J. Am. Chem. Soc.* **2000**, *122*, 2952; d) J. Larionova, G. Mathias, M. Pilkington, H. Andres, H. Stoeckli-Evans, H. U. Gudel, S. Decurtins, *Angew. Chem.* **2000**, *112*, 1667; *Angew. Chem. Int. Ed.* **2000**, *39*, 1605; e) R. J. Parker, L. Spiccia, K. J. Berry, G. D. Fallon, B. Moubaraki, K. S. Murray, *Chem. Commun.* **2001**, 333; f) V. Marvaud, J. M. Herrera, T. Barrilero, F. Tuyeras, R. Garde, A. Sculiller, C. Decroix, M. Cantuel, C. Desplanches, *Monatsh. Chem.* **2003**, *134*, 149.
[13] a) J. J. Sokol, A. G. Hee, J. R. Long, *J. Am. Chem. Soc.* **2002**, *124*, 7656; b) C. P. Berlinguette D. Vaughn, C. Cañada-Villalta, J. R. Galán-Mascarós, K. R. Dunbar, *Angew. Chem.* **2003**, *115*, 1561; *Angew. Chem. Int. Ed.* **2003**, *42*, 1523; c) H. J. Choi, J. J. Sokol, J. R. Long, *Inorg. Chem.* **2004**, *43*, 1606.
[14] a) O. Sato, T. Iyoda, A. Fujishima, K. Hashimoto, *Science* **1996**, *271*, 49; b) O. Sato, S. Hayami, Y. Einaga, Z. Z. Gu, *Bull. Chem. Soc. Jpn.* **2003**, *76*, 443.
[15] a) O. Sato, T. Iyoda, A. Fujishima, K. Hashimoto, *Science* **1996**, *272*, 704; b) A. Bleuzen, C. Lomenech, V. Escax, F. Villain, F. Varret, C. Cartier dit Moulin, M. Verdaguer, *J. Am. Chem. Soc.* **2000**, *122*, 6648; c) C. Cartier dit Moulin, F. Villain, A. Bleuzen, M. A. Arrio, P. Sainctavit, C. Lomenech, V. Escax, F. Baudelet, E. Dartyge, J. J. Gallet, M. Verdaguer, *J. Am. Chem. Soc.* **2000**, *122*, 6653; d) V. Escax, A. Bleuzen, C. Cartuer dit Moulin, F. Villain, A. Goujon, F. Varret, M. Verdaguer, *J. Am. Chem. Soc.* **2001**, *123*, 12 536; e) G. Champion, V. Escax, C. Cartier dit Moulin, A. Bleuzen, F. Villain, F. Baudelet, E. Dartyge, M. Verdaguer, *J. Am. Chem. Soc.* **2001**, *123*, 12 544.
[16] a) R. Lescouëzec, F. Lloret, M. Julve, J. Vaissermann, M. Verdaguer, R. Llusar, S. Uriel, *Inorg. Chem.* **2001**, *40*, 2065; b) R. Lescouëzec, F. Lloret, M. Julve, J. Vaissermann, M. Verdaguer, *Inorg. Chem.* **2002**, *41*, 818; c) L. M. Toma, R. Lescouëzec, L. D. Toma, F. Lloret, M. Julve, J. Vaissermann, M. Andruh, *J. Chem. Soc. Dalton Trans.* **2002**, 3171.
[17] a) H. Oshio, O. Tamada, H. Onodera, T. Ito, T. Ikoma, S. Tero-Kubota, *Inorg. Chem.* 1999, *38*, 5686; b) H. Oshio, H. Onodera, O. Tamada, H. Mizutani, T. Hikichi, T. Ito, *Chem. Eur. J.* **2000**, *6*, 2523; c) H. Oshio, M. Yamamoto, T. Ito, *Inorg. Chem.* **2002**, *41*, 5817.
[18] J. A. Smith, J. R. Galán-Mascarós, R. Clérac, J. S. Sun, X. Ouyang, K. R. Dunbar, *Polyhedron* **2001**, *20*, 1727.
[19] a) K. R. Klausmeyer, S. R. Wilson, T. B. Rauchfuss, *J. Am. Chem. Soc.* **1999**, *121*, 2705; b) S. M. Contakes, K. K. Klausmeyer, T. B. Rauchfuss, *Inorg. Chem.* **2000**, *39*, 2069.
[20] V. Jacob, G. Huttner, E. Kaifer, P. Kircher, P. Rutsch, *Eur. J. Inorg. Chem.* **2001**, 2783.
[21] D. J. Darensbourg, W. Z. Lee, M. J. Adams, J. C. Yarbrough, *Eur. J. Inorg. Chem.* **2001**, 2811.
[22] Z. N. Chen, R. Appelt, H. Vahrenkamp, *Inorg. Chim. Acta* **2000**, *309*, 65.
[23] a) J. L. Heinrich, P. A. Berseth, J. R. Long, *Chem. Commun.* **1998**, 1231; b) P. A. Berseth, J. J. Sokol, M. P. Shores, J. L. Heinrich, J. R. Long, *J. Am. Chem. Soc.* **2000**, *122*, 9655; c) J. J. Sokol, M. P. Shores, J. R. Long, *Angew. Chem.* **2001**, *113*, 242; *Angew. Chem. Int. Ed.* **2001**, *40*, 236; d) J. J. Sokol, A. G. Hee, J. R. Long, *J. Am. Chem. Soc.* **2002**, *124*, 7656; e) M. P. Shores, J. J. Sokol, J. R. Long, *J. Am. Chem. Soc.* **2002**, *124*, 2279; f) J. Y. Yang, M. P. Shores, J. J. Sokol, J. R. Long, *Inorg. Chem.* **2003**, *42*, 1403.
[24] R. Lescouëzec, J. Vaissermann, F. Lloret, M. Julve, M. Verdaguer, *Inorg. Chem.* **2002**, *41*, 5943.
[25] R. Lescouëzec, J. Vaissermann, C. Ruiz-Pérez, F. Lloret, R. Carrasco, M. Julve, M. Verdaguer, Y. Dromzee, D. Gatteschi, *Angew. Chem.* **2003**, *115*, 1521; *Angew. Chem. Int. Ed.* **2003**, *42*, 1483.

[26] a) A. Caneschi, D. Gatteschi, N. Lalioti, C. Sangregorio, R. Sessoli, G. Venturi, A. Vindigni, A. Rettori, M. G. Pini, M. A. Novak, *Angew. Chem.* **2001**, *113*, 1810; *Angew. Chem. Int. Ed.* **2001**, *40*, 1760; b) A. Caneschi, D. Gatteschi, N. Lalioti, R. Sessoli, L. Sorace, V. Tangoulis, A. Vindigni, *Chem. Eur. J.* **2002**, *8*, 286; c) R. Clérac, H. Miyasaka, M. Yamashita, C. Coulon, *J. Am. Chem. Soc.* **2002**, *124*, 12837; d) H. Miyasaka, R. Clérac, K. Mizushima, K. Sugiura, M. Yamashita, W. Wernsdorfer, C. Coulon, *Inorg. Chem.* **2003**, *42*, 8203; e) T. F. Liu, D. Fu, S. Gao, Y. Z. Zhang, H. L. Sun, G. Su, Y. J. Liu, *J. Am. Chem. Soc.* **2003**, *125*, 13976.
[27] L. M. Toma, R. Lescouëzec, F. Lloret, M. Julve, J. Vaissermann, M. Verdaguer, *Chem. Commun.* **2003**, 1850.
[28] R. Lescouëzec, J. Vaissermann, L. M. Toma, R. Carrasco, F. Lloret, M. Julve, *Inorg. Chem.* **2004**, *43*, 2234.
[29] a) R. Lescouëzec, G. Marinescu, J. Vaissermann, F. Lloret, J. Faus, M. Andruh, M. Julve, *Inorg. Chim. Acta* **2003**, *350*, 131; b) M. C. Muñoz, M. Julve, F. Lloret, J. Faus, M. Andruh, *J. Chem. Soc. Dalton Trans.* **1998**, 3125; c) S. Decurtins, H. W. Schmalle, R. Pellaux, P. Schneuwly, A. Hauser, *Inorg. Chem.* **1996**, *35*, 1451; d) F. D. Rochon, M. Melanson, M. Andruh, *Inorg. Chem.* **1996**, *35*, 6086.
[30] S. Jagner, E. Ljungström, N. G. Vannerberg, *Acta Chem. Scand.* **1974**, *28*, 623.
[31] M. Schwarten, D. Babel, *Z. Anorg. Allg. Chem.* **2000**, *626*, 1921.
[32] L. L. Merrit, E. D. Schroeder, *Acta Crystallogr.* **1956**, *9*, 801.
[33] I. Dance, M. Scudder, *Chem. Eur. J.* **1996**, *2*, 481.
[34] C. J. O'Connor, *Prog. Inorg. Chem.* **1982**, *29*, 203.
[35] A. Rodríguez-Fortea, P. Alemany, S. Alvarez, E. Ruiz, A. Sccuiller, C. Decroix, V. Marvaud, J. Vaissermann, M. Verdaguer, I. Rosenman, M. Julve, *Inorg. Chem.* **2001**, *40*, 5868.
[36] M. Verdaguer, *Polyhedron* **2001**, *20*, 1115.
[37] F. Lloret, R. Ruiz, M. Julve, J. Faus, Y. Journaux, I. Castro, M Verdaguer, *Chem. Mater.* **1992**, *4*, 1150.
[38] a) R. L. Carlin, *Magnetochemistry*, Springer, Berlin, **1986**, p. 148; b) D. Armentano, G. De Munno, F. Lloret, A. V. Palii, M. Julve, *Inorg. Chem.* **2002**, *41*, 2007; c) S. Ferrer, F. Lloret, I. Bertomeu, G. Alzuet, J. Borrás, S. García-Granda, M. Liu-González, J. G. Haasnoot, *Inorg. Chem.* **2002**, *41*, 5851; d) B. S. Tsukerblat, M. I. Belinskii, V. E. Fainzil'berg, *Sov. Sci. Rev. B Chem.* **1987**, *9*, 337.
[39] J. Cano, E. Ruiz, S. Alvarez, M. Verdaguer, *Comments Inorg. Chem.* **1998**, *20*, 27.
[40] J. Cano, Y. Journaux, *Magnetism: Molecules to Materials V* (Eds.: J. S. Miller, M. Drillon), Wiley, **2004**, Chapter 6.
[41] S. Homma, H. Matsuda, N. Ogita, *Prog. Theor. Phys.* **1986**, *75*, 1058.
[42] S. Miyazawa, S. Miyashita, M. S. Makivic, S. Homma, *Prog. Theor. Phys.* **1993**, *89*, 1167.
[43] J. C. Revee, *J. Chem. Educ.* **1985**, *62*, 44.
[44] A. Earnshaw, *Introduction to Magnetochemistry*, Academic Press, London, **1968**.
[45] A. D. Becke, *Phys. Rev. A* **1988**, *38*, 3098.
[46] C. Lee, W. Yang, R. G. Parr, *Phys. Rev. B* **1988**, *37*, 785.
[47] A. D. Becke, *J. Chem. Phys.* **1993**, *98*, 5648.
[48] GAUSSIAN 98, M. J. Frisch, G. W. Trucks, H. B. Schlegel, G. E. Scuseria, M. A. Robb, J. R. Cheeseman, V. G. Zakrzewski, J. A. Montgomery, R. E. Stratmann, J. C. Burant, S. Dapprich, J. M. Millam, A. D. Daniels, K. N. Kudin, M. C. Strain, O. Farkas, J. Tomasi, V. Barone, M. Cossi, R. Cammi, B. Mennucci, C. Pomelli, C. Adamo, S. Clifford, J. Ochterski, G. A. Petersson, P. Y. Ayala, Q. Cui, K. Morokuma, D. K. Malick, A. D. Rabuck, K. Raghavachari, J. B. Foresman, J. Cioslowski, J. V. Ortiz, A. G. Baboul, B. B. Stefanov, G. Liu, A. Liashenko, P. Piskorz, I. Komaromi, R. Gomperts, R. L. Martín, D. J. Fox, T. Keith, M. A. Al-Laham, C. Y. Peng, A. Nanayakkara, C. González, M. Challacombe, P. M. W. Gill, B. G. Johnson, W. Chen, M. W. Wong, J. L. Andres, M. Head-Gordon, E. S. Replogle, J. A. Polple, Gaussian, Inc., Pittsburgh, PA, **1998**.
[49] A. Schaefer, A. Horn, R. Ahlrichs, *J. Chem. Phys.* **1992**, *97*, 2571.
[50] A. Schaefer, C. Huber, R. Ahlrichs, *J. Chem. Phys.* **1994**, *100*, 5829.
[51] J. Cano, P. Alemany, S. Alvarez, M. Verdaguer, E. Ruiz, *Chem. Eur. J.* **1998**, *4*, 476.
[52] E. Ruiz, J. Cano, S. Alvarez, P. Alemany, *J. Am. Chem. Soc.* **1998**, *120*, 11122.
[53] E. Ruiz, J. Cano, S. Alvarez, P. Alemany, *J. Comput. Chem.* **1999**, *20*, 1391.
[54] J. Cano, E. Ruiz, P. Alemany, F. Lloret, S. Alvarez, *J. Chem. Soc. Dalton Trans.* **1999**, 1669.
[55] J. E. Carpenter, F. Weinhold, *J. Mol. Struct.* **1988**, *169*, 41.
[56] A. E. Reed, L. A. Curtis, F. Weinhold, *Chem. Rev.* **1988**, *88*, 899.
[57] F. Weinhold, J. E. Carpenter, *The Structure of Small Molecules and Ions*, Plenum, **1988**, p. 227.
[58] N. Walker, D. Stuart, *Acta Crystallogr.* **1983**, *A39*, 156.
[59] G. M. Sheldrick, SHELX-86, A Program for Crystal Structure Solution, University of Göttingen, Göttingen (Germany), **1986**.
[60] G. M. Sheldrick, SHELXL-97, A Program for Crystal Structure Solution, University of Göttingen, Göttingen (Germany), **1998**.
[61] L. J. Farrugia, *Appl. Crystallogr.* **1999**, *32*, 837.
[62] D. J. Watkin, J. R. Carruthers, P. W. Betteridge, CRYSTALS, Chemical Crystallography Laboratory, University of Oxford, Oxford (UK), **1996**, Issue 10.
[63] M. Nardelli, PARST95, *J. Appl. Crystallogr.* **1995**, *28*, 659.
[64] CRYSTALMAKER 4.2.1, CrystalMaker Software, Bicester, Oxfordshire, UK, **2001**.

Received: June 17, 2004
Published online: October 29, 2004

